ISEL – Instituto Superior de Engenharia de Lisboa

ADEETC – Área Departamental de Engenharia de
Electrónica e Teleconumicações e de Computadores

MEET
Mestrado em Eng. Electrónica e Telecomunicações
Dissertação

Self-Diagnosing and Optimization of Low Coverage and High Interference in 3G/4G Radio Access Networks

MARCO DÉCIO BAPTISTA SOUSA

Orientador(es)

Orientador: *Doutor*   Pedro Manuel de Almeida Carvalho Vieira

Co-orientador: *Mestre*   André Eduardo Ponciano Martins

Dezembro, 2016

Abstract

Self-Organizing Networks (SON) solutions have been developed and implemented in the last years as a Mobile Network Operator (MNO) strategy to deal with the complexity of current networks.

This research work, focuses on the self-optimization branch of SON solutions. It aims to empower a network with automatic capabilities for detecting and optimizing poor Radio Frequency (RF) performance scenarios.

The detection and optimization of those scenarios, is based on Drive Test (DT) data. This leads to the development of a DT classification model to assert the quality of data collected through DT for a given cell, as it supports all decision making in terms of detection and optimization of poor RF situations.

The DT model was calibrated with subjective testing in the form of inquiries made to fifty Radio Access Network (RAN) engineers.

Three algorithms were implemented for detection of low coverage and high interference scenarios. Besides identifying and dividing into clusters the DT data that denotes each problem, harshness metrics at cell and cluster level allow to identify the most severe situations.

Moreover, an antenna physical parameter optimization algorithm, based on a Particle Swarm Optimization (PSO) algorithm, is able to purpose new Electrical Downtilt (EDT), Mechanical Downtilt (MDT) or the antenna orientation to improve or fix the detected RF problems.

All algorithms were tested with real MNO DT data and network topology, mainly on urban scenarios, where the detection and optimization is more critical for MNO.

Regarding the detection algorithms, in urban scenario, it was established that the situations of high interference were more prevailing than the low coverage.

The antenna self-optimization algorithm achieved an average gain of 78% on the tested cases.

Keywords: LTE, UMTS, SON, Coverage Detection, Interference Control, Tilt Optimization

Resumo

As redes SON têm sido, cada vez mais, uma das fortes apostas por parte das operadoras móveis para fazer face a crescente complexidade das redes móveis.

Este trabalho de pesquisa foca-se no ramo, das redes SON, de optimização automática. O objectivo é dotar uma rede móvel de capacidades de detecção e optimização de situações de má performance rádio.

Tendo em conta que toda a detecção e optimização é baseada em dados recolhidos por DT, surgiu a necessidade de desenvolver um modelo de qualidade para DT. Este modelo é usado como referência em termos de qualidade de dados disponíveis, para cada célula analisada.

O modelo de qualidade de DT foi calibrado através de questionários subjectivos, realizados a cinquenta engenheiros rádio.

Foram implementados três algoritmos para detecção de situações de má cobertura e interferência. Além de identificar e dividir em *clusters* os dados de DT com cada um dos problemas mencionados, as métricas de gravidade ao nível do *cluster* e da célula, permitem identificar os cenários mais graves.

Em termos de optimização, foi desenvolvido e implementado um algoritmo de optimização de tilts eléctrico e mecânico ou a orientação da antena, com base num algoritmo PSO.

Todos os algoritmos foram testados com dados reais de DT e de topologia de rede, principalmente em cenários urbanos.

No que diz respeito aos algoritmos de detecção, em cenário urbano, foi concluído que as situações de excesso de interferência são mais abundantes do que as situações de má cobertura.

O algoritmo de optimização dos parâmetros físicos de antenas, para os casos testados, obteve um ganho médio de 78%.

Palavras-chave: LTE, UMTS, SON, Deteção de cobertura, Controlo de interferência, Optimização de tilts

iv

Acknowledgments

A master thesis dissertation is the culmination of many years of study, effort and dedication. But it would not be possible without the valuable contribute and support that i have received throughout and where i stated my appreciation and gratitude.

To Celfinet that provided me with resources, support and valuable data to develop my research.

To the New Solutions team at Celfinet where i meet excellent professionals and friends.

To engineer André Martins for the constant accompaniment and help given since the first day of the project.

To engineer Pedro Vieira for the opportunity, for the invaluable guidance, support and time dedicated throughout the all work.

To my girlfriend that accompanied me and backed me up in the completion of this work.

And finally to my family, especially to my father and mother who have always provided with the conditions and support in the pursue of my goals.

vi

To my parents.

Contents

List of Tables

List of Figures

Acronyms

2G 2nd Generation. 2

3G 3rd Generation. 2, 5, 11, 13, 22–24, 43, 46, 61, 66

3GPP 3rd Generation Partnership Project. 2, 23, 59

4G 4th Generation. 2, 22, 23, 26, 43, 46, 61, 72

5G 5th Generation. 2

API Application Programming Interface. 33

BCCH Broadcast Control Channel. 21

BPSK Binary Phase-Shift Keying. 19

BS Base Station. 6, 9–11, 15–17, 20, 23

CapEx Capital Expenditure. 2

CCCH Common Control Channel. 21

CCO Coverage and Capacity Optimization. 3

CDF Cumulative Density Function. 81

CDMA Code Division Multiple Access. 19, 26

CDR Call Drop Rate. 40

CM Communication Management. 12

CN Core Network. 9, 11–16, 22, 40

CS Circuit Switch. 11

CSSR Call Setup Success Rate. 40

CTCH Common Traffic Channel. 21

DCCH Dedicated Control Channel. 21

DT Drive Test. i, iii, 3, 4, 29–36, 39–41, 44–47, 49, 50, 57, 61–67, 69, 70, 80, 82, 84, 85

DTCH Dedicated Traffic Channel. 21

E-UTRAN Evolved Universal Terrestrial Radio Access Network. 22–24

EcIo Energy per chip to Interference Ratio. 46, 69, 70

EDGE Enhanced Data rates for GSM Evolution. 2

EDT Electrical Downtilt. i, 57, 73, 76, 79

eNB evolved NodeB. 23–25

EPC Evolved Packet Core. 22–25

FDD Frequency-Division Duplexing. 19

GPS Global Positioning System. 40

GSM Global System for Mobile Communications. 2

HetNet Heterogeneous Networks. 2

HSPA High Speed Downlink Packet Access. 2

HSS Home Subscriber Server. 25

IoT Internet of Things. 2

KPI Key Performance Indicator. 40

LoS Line-of-Sight. 8, 70–72, 75, 76

LTE Long Term Evolution. 2, 4, 5, 9, 22–25, 65, 66, 84

MDT Mechanical Downtilt. i, 57, 73, 76, 79

ME Mobile Equipment. 11

MM Mobility Management. 12

MME Mobility Management Entity. 23–25

MNO Mobile Network Operator. i, 2, 9, 10, 84

MRM Measurement Report Messages. 40

MS Mobile Station. 6, 11

MT Mobile Termination. 13

NB NodeB. 24

NLoS Non-Line-of-Sight. 7, 8, 69

OFDM Ortoghonal Frequency Division Multiplexing. 4, 25–27

OFDMA Orthogonal Frequency-Division Multiple Access. 25

OpEx Operating Expense. 2

OSI Open Systems Interconnection. 13

OSM Open Street Map. 33

OSS Operational Support System. 40

P-GW Packet Data Network Gateway. 23, 25

PCCH Paging Control Channel. 21

PCRF Policy Control and Charging Rules Functions. 25

PS Packet Switch. 11

PSC Primary Scrambling Code. 16, 18

PSO Particle Swarm Optimization. i, iii, 51, 53–55, 57–59

QoS Quality of Service. 9, 11, 13, 14, 16, 17, 25, 80

RAB Radio Access Bearers. 14, 17

RAN Radio Access Network. i, 5, 9, 11, 40, 85

RAT Radio Access Technology. 33

RB Radio Bearer. 16

RF Radio Frequency. i, 3, 4, 9, 29, 33, 39, 40, 46, 59, 60, 75, 80–82, 84, 85

RNC Radio Network Controller. 11, 15–18, 20, 23, 24

RNS Radio Network Subsystem. 11, 15, 16

RRM Radio Resource Management. 11, 12, 16, 24

RSCP Received Signal Code Power. 43, 45, 59, 67, 69, 70

RSRP Reference Signal Received Power. 43, 45, 59, 72, 74, 75

RSRQ Reference Signal Received Quality. 46, 72, 74, 75

S-GW Serving Gateway. 23–25

SINR Signal-to-Interference plus Noise Ratio. 17

SON Self-Organizing Networks. i, iii, 2, 29, 39, 82, 84, 85

TDD Time-Division Duplexing. 19

TDMA Time Division Multiple Access. 26

TRX Transmitter-Receivers. 16

UE User Equipment. 11–16, 18, 20–25, 40

UMTS Universal Mobile Telecommunications System. 2, 4, 5, 9, 11–14, 65, 84

USIM UMTS Service Identity Module. 11, 24

UTRAN UMTS Terrestrial Access Network. 11–17, 22–24

VMR Variance to Mean Ratio. 32

WCDMA Wideband Code Division Multiple Access. 4, 15, 17–20

Chapter 1

Introduction

This chapter describes the scope of this project. The motivation that led to its development is presented, as well as the objectives to be accomplished. It is outlined this document structure and finally are presented the publications that outcome this project.

1.1   Motivation

The current mobile networks provide service to an all time record of sub-scribers. The total number of mobile subscriptions, in the first quarter of 2016, was around 7.4 billion. The number of subscriptions will keep growing on average 3% year-on-year, specially supported by the developing markets [3].

Regarding the radio access technology, Global System for Mobile Com-munications (GSM) and Enhanced Data rates for GSM Evolution (EDGE) presently represents the largest share of mobile subscriptions, nonetheless the tendency is to be gradually substituted by Universal Mobile Telecom-munications System (UMTS)/High Speed Downlink Packet Access (HSPA) and Long Term Evolution (LTE). In 2015, LTE subscribers reached the first billion and by 2021 is expected to reach 4.3 billion [3].

As for mobile data traffic, it continues to grow at impressive rates. Data traffic grew 60% between the first quarter of 2015 and the first quarter of 2016, from almost 4 exabyte per month to around 5.5 exabyte per month, remembering that 1 exabyte are 1 073 741 824 gigabytes. The growth in mo-bile data traffic is due to the rising number of smartphones subscriptions and the increasing data consumption per subscriber. As smartphones continue to gain market share, it is expected to aid the growth of data traffic.

Currently, a mobile network operator, normally manages in parallel both a 2nd Generation (2G), a 3rd Generation (3G) and a 4th Generation (4G) network. Moreover, by the end of this decade the deployment of the first 5th Generation (5G) networks, massive Internet of Things (IoT) and more complex Heterogeneous Networks (HetNet) are expected.

The key point, is that MNO are under pressure to run networks increas-ingly more complex, and at the same time to offer more service, to more sub-scribers. All this maintaining or decreasing both Operating Expense (OpEx) and Capital Expenditure (CapEx).

In order to handle these challenges, the concept of SON was introduced within Release 8 of 3rd Generation Partnership Project (3GPP). The SON can be defined as a set of use cases that govern a network, including the planning, set up and maintenance activities. In this way a network is able to manage its resources to obtain greater performance at any time.

A SON can operate mainly on three areas: self-configuration, self-optimization

and self-healing. Self-configuration aims to turn a base station essentially a "plug and play" element. This reduces the manual intervention needed and the error chance in the base station deployment process, thereby saving costs and increasing reliability. Self-optimization includes automatic Coverage and Capacity Optimization (CCO), load balancing and traffic steering, energy saving routines and other optimization process. Self-healing routines are triggered when a system fault occurs. It tries to decrease the effects on the users by, for instance, increasing the boundaries of the adjacent cells.

1.2 Objectives

This work aims to develop, implement and test a self-optimization algorithm. Its goal is to detect poor RF conditions related to bad coverage or related to high interference scenarios, based on DT data and network topology information. Moreover, the detection process must identify which cells denote RF issues.

After the detection of the above-mentioned scenarios, an antenna physical parameter optimization algorithm should be implemented. Its objective is to propose a new set of parameter that minimizes or fixes the detected problems.

This work was developed under a partnership with Celfinet, a Portuguese telecommunications consulting company, which provided DT data and network topology information, as well as valuable guidance and support. About the duration on this research work it started on April 2015.

1.3 Publications

During the execution of this master thesis work several articles were submitted and presented in conferences:

Marco Sousa, André Martins, Pedro Vieira, Nuno Silva, António Rodrigues. *Caracterização da Fiabilidade de Medidas Rádio em Larga Escala para Redes Auto-otimizadas.* 9.º Congresso do Comité Português da URSI - "5G e a Internet do futuro", 2015.

Marco Sousa, André Martins, Pedro Vieira. *Self-Diagnosing Low Coverage and High Interference in 3G/4G Radio Access Networks based on Automatic RF Measurement Extraction.* 13th International Conference on Wire-

less Networks and Mobile Systems (WYNSIS), 2016. **(Best Student Paper Award)**

Marco Sousa, André Martins, Pedro Vieira. *Self-Optimization of Low Coverage and High Interference in Real 3G/4G Radio Access Networks.* 13_{th} Conference on Electronics, Telecommunications and Computers (CETC), 2016.(submitted)

1.4   Thesis Structure

The work is organized in six chapters. Chapter 1 introduces the current master thesis work, namely its motivations, objectives and published work.

Chapter 2 is the state of art chapter. It is constituted by an overview of radio communications, fundamental concepts, an introduction to UMTS and LTE and its radio access technologies: Wideband Code Division Multiple Access (WCDMA) and Ortoghonal Frequency Division Multiplexing (OFDM).

Chapter 3, exhibits a new DT classification model to assert DT quality. The model is based on the DT data dispersion and the covered level of the road/street network.

Chapter 4, presents the self-diagnosis developed algorithms, the coverage holes, overshooting and pilot pollution. The detection work flow is detailed for the three algorithms. It also contains the self-optimization algorithm which optimizes antenna physical parameters configuration to minimize or fix eventual RF performance issues.

In Chapter 5, the data analysis from the DT reliability model, the self-diagnosis algorithms and the antenna self-optimization algorithm are presented. Finally, in Chapter 6 the work main conclusions are drawn.

Chapter 2

State of the Art

This chapter presents the state of the art and the theoretical knowledge that supported the development of the current work. It highlights some mobile communications basic concepts. Then, an overview of the UMTS network, along with a description of the network architecture and the 3G RAN is performed. Finally, the LTE is also presented, highlighting its architecture and its RAN.

2.1   Radio Communication Fundamentals

In 1896, Marconi used the "Hertzian" wave to communicate, inventing this way the first wireless communication system of the history. The use of radio waves for transmitting information is the base of all radio communications.

2.1.1   Radio Propagation

The fundamental principle of radio propagation is that utilizes radio waves as a transmission medium. These are results of electromagnetic fields, that under certain circumstances, generate waves that radiate from the source to the surrounding environment. These radio waves, are strongly dependent on the propagation environment. As a consequence, a radio communication system is vulnerable to the environment as mountains, rivers, buildings, the atmosphere and so on.

The simplest radio communication system, consists of two elements, which are the transmitter and the receiver. But, in mobile networks, for instance, these two elements are combined in one single element called a transceiver. This allows for a device to behave both as a transmitter and receiver. Assuming, that a Base Station (BS) acts as a transmitter, the generated radio signal will propagate to a Mobile Station (MS). The received signal strength, is dependent, on the distance to the transmitter, the carrier frequency, bandwidth and the propagation environment. Any artificial or natural obstacles like buildings, terrain profile, weather conditions, etc., strongly affects the way and time of signal propagation. In addition, parameters as the transmitter height and beam direction actively affects the propagation distance, mode and delay.

Nonetheless, there are three main problems with radio communications: multipath phenomenon, fading and radio resource scarcity. Multipath occurs in consequence of the radio propagation wide diversity, dynamism and the existence of several propagation mechanisms, such as reflection, diffraction and scattering phenomena, as shown in Figure 2.1.

The after-effect of multipath are fluctuations in the received signals characteristics, including phase, amplitude and angle of arrival, giving rise to multipath fading. Reflection occurs when a radio wave collides with an obstruction whose dimensions are much larger than the signal wavelength. The
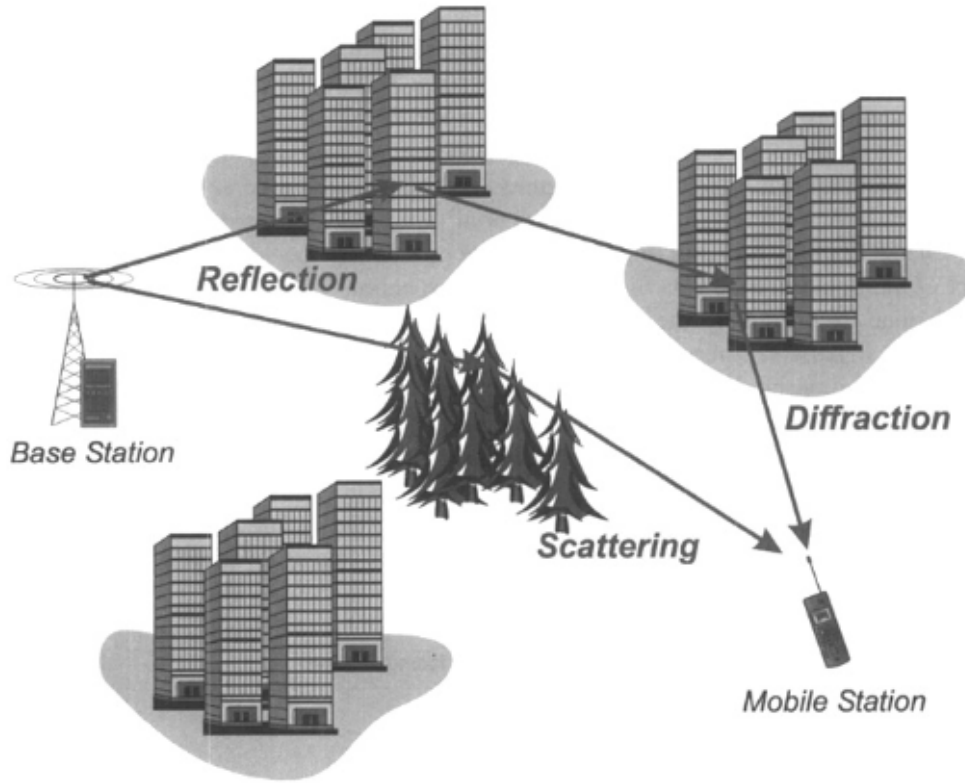
Figure 2.1: Radio propagation mechanisms [11].

follow-up, is a reflect wave that will propagate in a new direction. Diffraction, also called shadowing, results from the collision of the radio wave with an obstacle, but instead of being reflected, the radio wave tends to travel around them, based on the Huygens principle. When the radio wave encounters obstacles whose dimensions are close to the radio wavelength, it is when scattering appears. Interestingly, these phenomena allow Non-Line-of-Sight (NLoS) radio communications. The downside, is that multipath leads to signal time dispersion and multipath fading. To minimize it, there are signal processing techniques specifically targeted to deal with these phenomena.

There are mainly two different ways of modeling the above-mentioned effects: link budget and time dispersion. Link budget essentially, estimates the received signal strength, in a specific location from a transmitter. It is achieved by estimating the path-loss, between the interest points, using radio channel propagation models. These models try to take into account the

several propagation constraints, mentioned so far. For the effect of multipath to be fully characterized, time dispersion should be considered. This can be done by estimating the different time delays of each replica of the transmitted signal. So, the signal will reach the receiver not only via direct path but also as a result of multipath replicas, and the overall signal received is a sum of the different signals that reach the mobile terminal. Each signal replica, as it has a different path length, will be added or subtracted from the total depending on its relative phases. This can lead to phase distortion and inter-symbolic interference when transmissions are made.

Figure 2.2 illustrates the main fading types that may arise in any radio network. The first main division introduces the large-scale fading class and
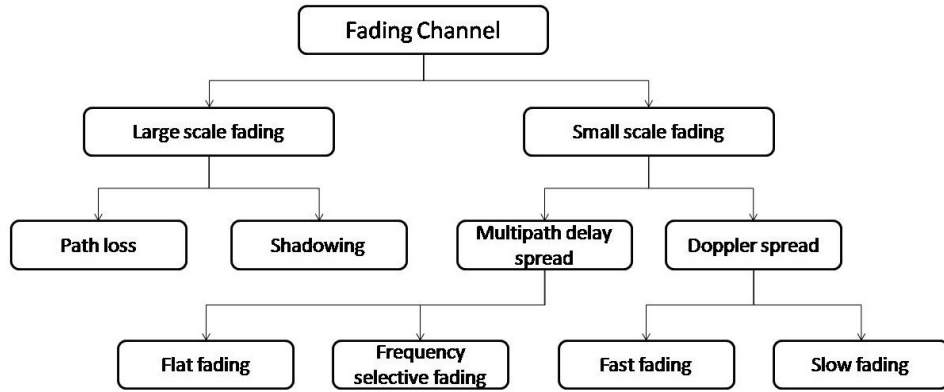
Figure 2.2: Radio channel classifications. Adapted from [6]

the small scale fading class. On one hand, the large-scale fading includes the concepts of path loss and shadowing, which are largely correlative with the user position, in relation to the transmitter, and its mobility pattern. On the other hand, small-scale fading, is the result of rapid variations in signal amplitude and phase. Small-scale fading that is also called Rayleigh fading or Rician fading, depending on NLoS or Line-of-Sight (LoS) existence.

Due to multipath delay spread, both flat fading or frequency selective fading can occur. The coherence bandwidth measures the separation in frequency after which two signals will experience unrelated fading. So, in flat fading, the coherence bandwidth of the channel is larger than the bandwidth of the signal. Therefore, all frequency components of the signal are exposed

to the same magnitude of fading. When the coherence bandwidth of the channel is smaller than the signals bandwidth, frequency selective fading occurs, as different frequency components will experience a different fading magnitude.

The channel coherence time of a channel sets the maximum time for that amplitude and phase changes stay correlated. So, slow fading arises when the channel time coherence is larger than the application delay requirements. In this circumstance, the amplitude and phase changes imposed by the channel can be considered roughly constant over a period of use. On the other side, when the coherence time of the channel is smaller relative to the delay requirements of an application, there are amplitude and phase changes imposed by the channel. The time coherence of a channel is related to the Doppler spread, which is caused by variations on the users speed.

In addition to fading and multipath, interference is a problem for every radio communication system. The dominant cause of interference is related with the limitation of RF resources. Due to that, some systems must reuse common radio resources, as in UMTS and LTE. In case of improper radio resource reuse, within this systems, it can lead to interference scenarios.

2.1.2 Cellular Radio Communication

The cellular concept was developed to provide duplex communication and to guarantee coverage and minimum Quality of Service (QoS) everywhere. Moreover, the spectrum use should be as more efficient as possible, to provide service to an increasing number of users. Thus, a cellular network is divided in sub-areas called cells. Each one, has its own BS and produces a radio link that will serve an amount of users, by emitting a low-level transmitted signal.

The basic architecture of any cellular based radio system, consists of a RAN and a Core Network (CN) for backbone transmission.

The cellular concept besides dealing with the above-mentioned issues, creates its own new issues though. It includes, intra-cell and inter-cell interference, due to the cellular structure, problems due to mobility and cell based radio resource scarcity.

The radio resources, in the matter of bandwidth, are limited and very expensive for MNO. This forces that bandwidth resources must be used in a

very efficient manner. Therefore, the concept of frequency reuse is employed, consisting on the attribution of different frequencies to each cell in a cluster. Then, this cluster pattern is reused for all the remaining network. Figure 2.3 exhibits this concept with one-seven and one-one frequency reuse patterns. In this case, a cellular system where radio bandwidth is reused, each BS
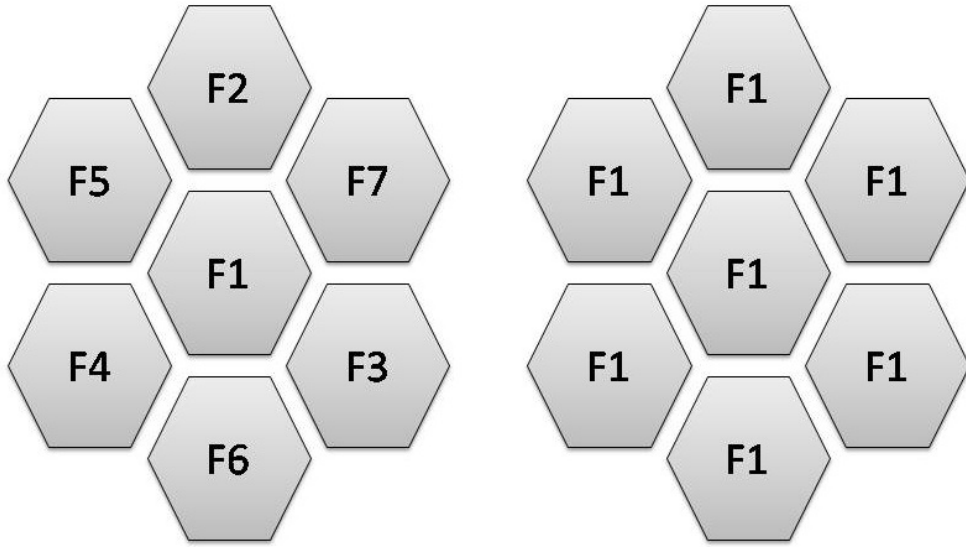
Figure 2.3: Frequency reuse patter. FR = 7 and FR = 1.

not only receives interference from mobiles in the home cell but also from terminals and BS from neighboring cells. Hence, depending on the source of interference, they can be classified as intra-cell interference (own cell) or inter-cell interference (other cells). So that these issues are minimized, the frequency reuse factor, which defines the re-utilization distance for the same frequency, is a critical planning parameter in any cellular system.

The cellular concept combined with frequency reuse increases the radio system capacity. Moreover, the smaller the cells, the more efficiently the radio spectrum is used. But, also, the network maintenance cost for MNO increases, as more BS are needed.

Another common practice in MNO, is to use multilayer networks combined with different cell types (macro, micro, pico). It allows to, depending on each location, to either increase capacity (hot spots) or focus on coverage

(rural areas). These solutions, however, set new requirements for handling the mobiles mobility and provide QoS everywhere.

Within the cellular network, a mobile equipment, must be reachable anywhere, anytime. For that purpose, operations such as, handover, location update and paging enable user mobility. Handover mechanism guarantees that when the user moves from one cell service area to another cell service area, its session is not lost, but forwarded to the new cell. When the mobile equipment is not in continuous communication with the BS, the location update (initiated by the MS) and the paging (initiated by BS) guarantees that the MS can be reached.

2.2 Universal Mobile Telecommunications System

In this section an overview over the UMTS and the Radio Resource Management (RRM) architecture is presented and a short description of the UMTS services and bearers is given.

2.2.1 Architecture

The UMTS network structural architecture is highlighted in Figure 2.4. A UMTS network can be divided in three main domains: the User Equipment (UE) domain, UMTS Terrestrial Access Network (UTRAN) and CN.

The 3G network terminal is called UE, being composed by the Mobile Equipment (ME) and the UMTS Service Identity Module (USIM), that is used to provide security features.

The subsystem that controls the wideband radio access, generally designated RAN, in the case of a UMTS network is designated as UTRAN. The UTRAN is divided in several Radio Network Subsystem (RNS) (see Figure 2.4). One RNS incorporates a set of radio elements, designated by NodeBs, and their controlling element, the Radio Network Controller (RNC). The RNSs are then connected to each other over the interface Iur.

The CN accommodates the remaining network elements needed for switching/routing and subscriber control. It incorporates the Circuit Switch (CS), the Packet Switch (PS) domains and the Registers. The last maintain static
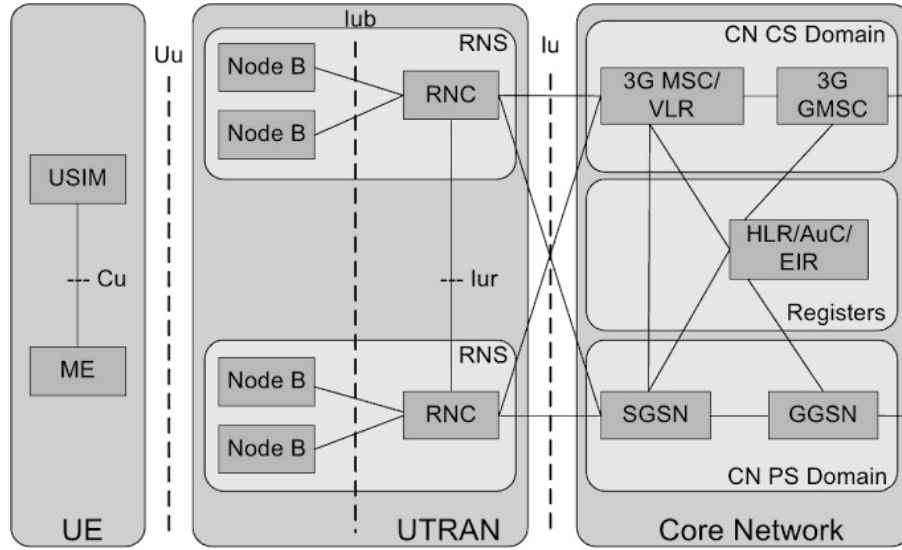
Figure 2.4: UMTS network architecture [10].

subscription and security information.

The are two main open interfaces in the UMTS network, the Iu, which is located between the UTRAN and the CN and the Uu between the UE and the UTRAN.

2.2.2   Resource Management Architecture

Taking into account the three main domains, explained above, and decomposing an UMTS network in its different responsibilities, the network main functionalities are evidenced, as illustrated in Figure 2.5. The responsibilities of user connection management is assigned to the Communication Management (CM) layer. Then, CM can be divided in sub-areas such as session management for the packet connection, call handling for circuit switched connections, as well as other services as short message systems.

Mobility Management (MM) encompasses all the functionalities related to mobility and security. For instance, operations such as location updates, fall within the MM.

Concerning the RRM, they are all the UTRAN algorithms which manages radio resources. Power control, handover management or admission control are some UTRAN algorithms.
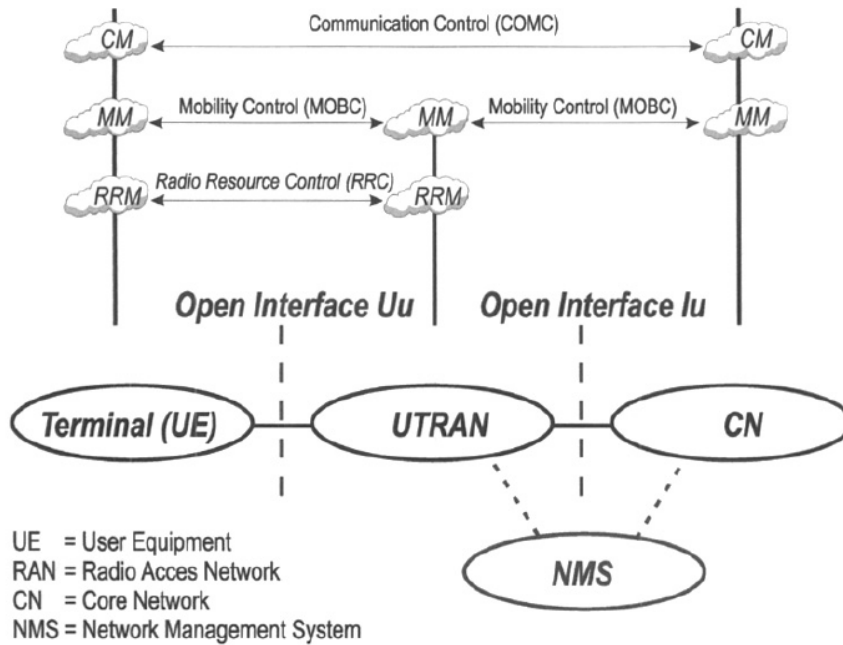
Figure 2.5: UMTS managements tasks and control duties [6].

2.2.3 Services and Bearer Architecture

A service bearer can be defined as a link between two points, which complies with a set of characteristics. Whenever a UE is being provided by any service, this service requires a minimum QoS specification. This specifications, guaranties that the user can access the required service. The bearer service specifies the configuration for Open Systems Interconnection (OSI) model layer two and physical layer, in order to have its QoS clearly defined. So, radio bearers are channels offered by layer two to higher layers for the transfer of user or control data.

In a UMTS network the end-to-end service requirements are divided into three entities: local bearer service, UMTS bearer service and external bearer service, as showed in Figure 2.6. The local bearer service contains all the mechanisms on how the end-user service is mapped between the terminal equipment and the Mobile Termination (MT). Then, the UMTS bearer service, gathers on the UTRAN and CN, several mechanisms allocate QoS over the UMTS/3G network. The last bearer, the external bearer service, deals
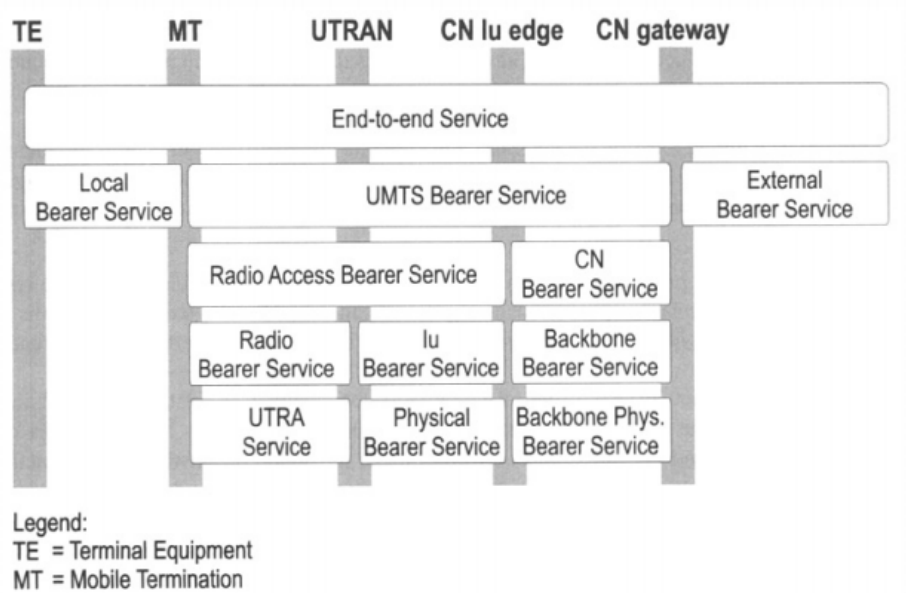
Figure 2.6: UMTS network bearer architecture [6].

with the QoS requirements for the external networks.

Within the UMTS network, the QoS handling differs in the UTRAN and the CN. This division between radio access bearer and CN bearer is required since the QoS requirements must be met in two different environments. For instance, the UTRAN service bearer, experiences several changes in function of time and user's mobility which presents itself as a challenge to maintain a certain QoS requirement. In opposition, the CN service bearer is quite constant. This is due, to the fact, that the backbone communication, through physical connections, are quite stable, countering the radio communications in the UTRAN. This division, pursues also, one of the UMTS network main goals i.e., the independence of the entire network infrastructure from the radio access technology.

2.3   UMTS Terrestrial Radio Access Network

The main objective of the UTRAN is to create and maintain Radio Access Bearers (RAB) between the UE and the CN. From the CN point of view, is as if it is directly connected to the UE. Being all radio communication aspects and configurations handled by the UTRAN, it assures that the required QoS

for the any given service, is met. Besides, this layered structure allows to encapsulate all the radio aspects in UTRAN. This is advantageous because later it can be modified or even replaced without changing the whole system.

2.3.1 UTRAN Architecture

The UTRAN consists of several RNS and each contains various BS (node B's) and one (or more) RNCs, as shown in Figure 2.7. The RNS connects
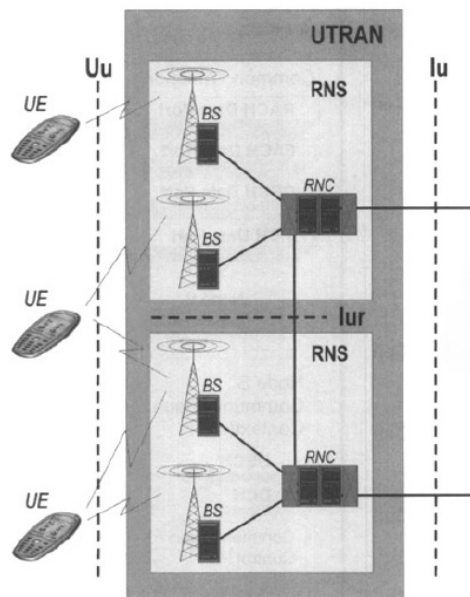
Figure 2.7: UTRAN architecture [6].

to the UE through the Uu interface. Furthermore, it communicates to the CN domains using the Iu interface. Finally, each RNS connects to each other using the open interface Iur, which carries both signaling and traffic information.

2.3.2 Base Station

Regarding the BS type, its main tasks are to establish the physical implementation of the Uu interface and the Iub interface. Regarding the Uu interface, the BS implements WCDMA radio access and maps the user data and signaling into the WCDMA physical channels, to communicate with the UE.

Moreover, a BS is constituted by several logical entities called cells. A cell is the smallest radio network entity that is unequivocally identified by an identification number, the cell id. The logical entity cell, has its physical counterpart, which is called a sector. Typically, a BS is configured with three sectors/cells, providing radio coverage all around the BS.

Every cell has one Primary Scrambling Code (PSC), which is attributed to the UE when it connects to a cell. Therefore, an UE uses both the scrambling code and the cell id to recognize a cell. Each cell, may have several Transmitter-Receivers (TRX), also called carriers, under it. One TRX maintains physical channels through the Uu interface and this carries the transport channels that contain the actual information, allowing communications between the network and the UE. Essentially, a TRX converts data flows from the terrestrial Iub connection to the radio path and vice-versa.

2.3.3   Radio Network Controller

The RNC performs both the switching and the controlling functions of the UTRAN. It is located between the interfaces Iub and Iu, connecting the UE to the CN. There is also a third interface, the Iur for inter-RNS connections.

The functionalities of a RNC can be classified into two parts, the UTRAN RRM and control functions. The RRM encompasses a collection of algorithms which aim to maintain the stability of the radio paths and the QoS of radio connections. The UTRAN control functions include all functions related to set-up, maintenance and release of the Radio Bearer (RB)s.

The RRM runs such algorithms as the handover control, power control, admission control, packet scheduling and code management.

Handover Control   Handover mechanisms provide mobility to a user in a mobile communications network. In this way is possible to maintain a traffic connection to a moving subscriber. The basic concept behind the handover, is to set up a new connection to a new cell, when a user moves from one coverage cell area to a new cell coverage area, and releasing the connection with the old cell. Regarding the criteria to trigger a handover it is mainly dependent on the handover strategy implemented in the system. However, most handover criteria are based on the signal quality, user mobility, traffic distribution and bandwidth.

In what concerns the handover types, there are two: hard-handover and soft-handover. During the hard-handover process the old connection is released before making the new connection. This very short cut in the connection is imperceptible for the user. In addition, the hard-handover can be performed between cells of different frequencies (inter-frequency), between cells of the same frequency (intra-frequency) and between cells of different technologies (inter-tech). In the case of the soft-handover, a new connection is established before releasing the old connection. In the WCDMA system, the majority of the handovers is intra-frequency soft handover.

A particular case of soft handover, is the softer handover. This occurs when a new signal is either added or removed from the active set which are under the same BS.

Power Control Power control is an essential feature of any WCDMA based cellular system. In WCDMA systems, which are interference limited multiple access systems, power control is used mainly to reduce intra-cell interference. Power control aims at adjusting every transmitter power so that it's only enough to provide the required QoS and minimize interference for other users. Also, power control is important to overcome the instability of the radio channel propagation characteristics. Without it, phenomena like fading and interference, drive down the system stability and ultimately degrades the quality of the user service. Moreover, the system capacity is maximized if the transmitted power of each transmitter is controlled so that its signal arrives to the BS with the minimum Signal-to-Interference plus Noise Ratio (SINR).

Admission Control and Package scheduler The task of the admission control is to estimate if a new call can have system access without compromising the bearer requirements of the other calls. Based on the admission control, the RNC either grants or rejects access. Also, the admission control is responsible for scheduling the packet sessions, based on the system capacity and the packet session characteristics, such as the number of packet call per session, reading time as well as the number of packets per call. So, the admission control is responsible for keeping the QoS of the accepted RAB and controlling their influence to the UTRAN performance.

Code Management   The RNC is responsible for the management of both the channelization and PSC used in the Uu interface. Every cell uses one PSC which allows the UE to make a separation between cells, by recognizing this code. In turn, under every PSC, the RNC has a set of channelization codes. These codes are used for channel separation when a UE establishes a connection with the network. Any data sent on the Uu interface is coded using the scrambling and channelization code.

2.3.4   Wide Code Division Multiple Access

From the radio resources standpoint, it is crucial how they are allocated to simultaneous users. Hence, this management is one of the most crucial features of any radio communication system.

The main aspect of multiple access techniques, which enables to provide service to simultaneous users, is how the available frequency band is allocated. In case of WCDMA, which stands for Wideband Code Division Multiple Access, it is a spread-spectrum-based radio access scheme. So, the radio resources are allocated based on codes. Thus, all the simultaneous users can occupy the same bandwidth at the same time, as presented in Figure 2.8.
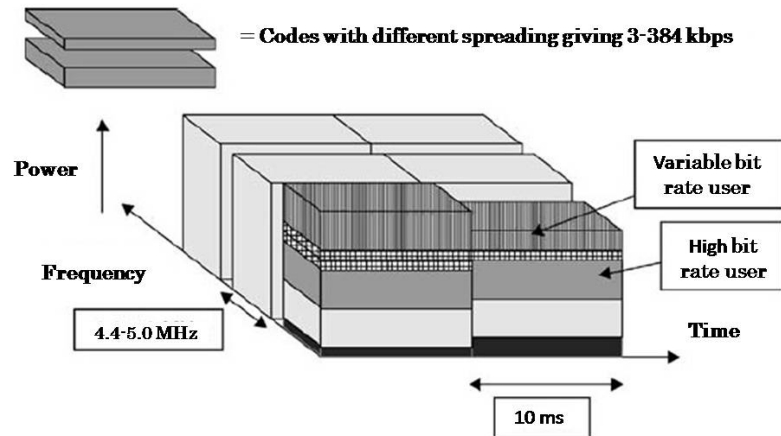
Figure 2.8: Wide code division multiple access [11].

In WCDMA, user information bits are spread over a wide bandwidth by multiplying user data by quasi-random bits (called chips) derived from the Code Division Multiple Access (CDMA) codes. The use of variable spreading codes may increase or decrease the bit rates. The chip rate of 3.84 Mcps leads to a carrier bandwidth of 5 MHz.

From Figure 2.8, it can be asserted that the user data rate is kept constant during each 10 ms frame. Nonetheless, the data capacity between users can change from one frame to another frame. This allows a fast radio capacity allocation, which is controlled by the network to achieve optimal throughput at any time.

In WCDMA, Time-Division Duplexing (TDD) and Frequency-Division Duplexing (FDD) is supported. In FDD two carriers of 5 MHz are used for uplink and downlink respectively. In TDD, one carrier of 5 MHz is shared between both uplink and downlink, using time slots.

Spreading and Despreading   Let us assume a Binary Phase-Shift Keying (BPSK) modulated bit sequence of rate R. A spreading operation corresponds to the multiplication of the user data by a sequence of 8 code bits, called chips. We observe, in Figure 2.9 that the resulting spread data is at a rate of $8 \times R$. In this case, it would be said that a spreading factor of 8
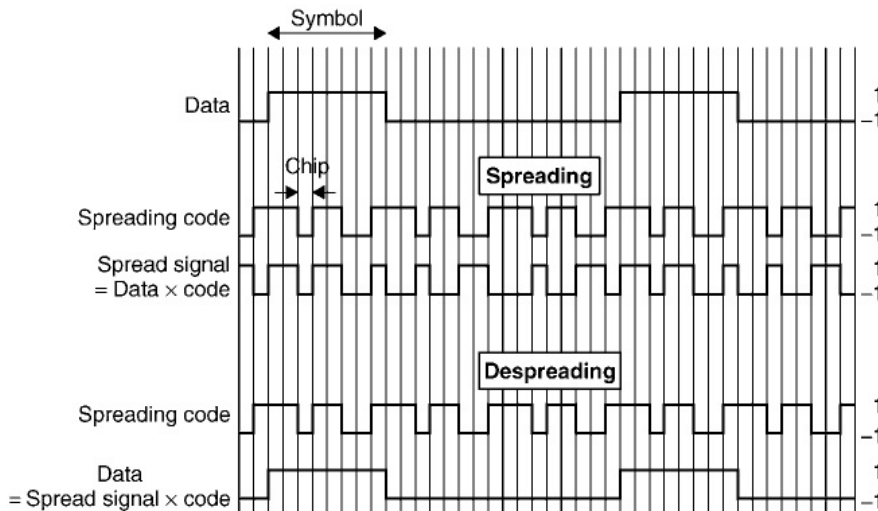
Figure 2.9: Spreading and despreading in CDMA [11].

was used. This wideband signal would then be transmitted, to the receiver, across a wireless channel.

In despreading, the spread user data is again multiplied by the very same sequence of 8 code chips. As shown in Figure 2.9, the original user data is recovered.

The increased of the signaling rate by a factor of 8, in this example, corresponds to a widening of the occupied spectrum of the user data signal.

Radio Channels   The WCDMA uses a three layer channel organization scheme, namely the logical channels, transport channels and physical channels (see Figure 2.10). Therefore, the logical channels describe the type of
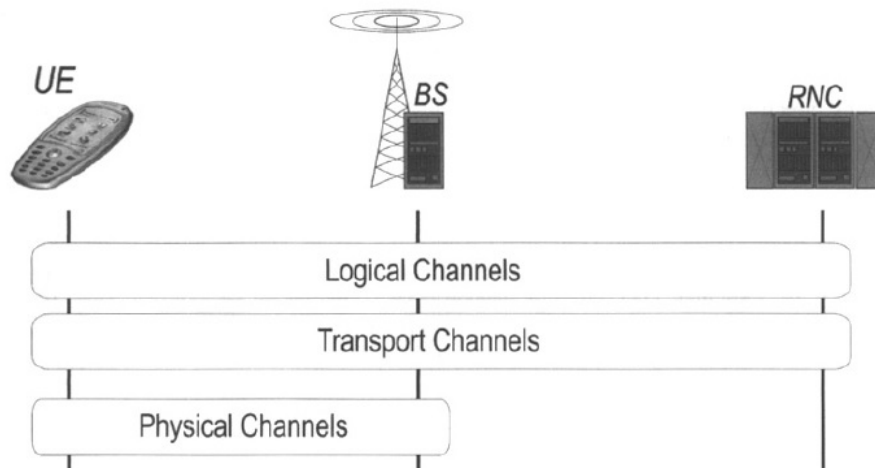
Figure 2.10: Channel types in UTRAN [6].

information, the transport channels describe how the logical channels are to be transmitted and the physical channels, provide the physical medium to the transmission.

From the RNC point of view, it only "sees" the logical and transport channels. The physical channels provide data transmission over the Uu interface, whereas only the UE and the BS interact.

Regarding the logical channels, they can be understood more like different types of tasks that the network must perform, than actual channels themselves. Such tasks, as informing the UE about cell codes, neighbor lists

and general information are provided through the logical channel Broadcast Control Channel (BCCH). The Paging Control Channel (PCCH) is used for paging the UE. The Common Control Channel (CCCH) is used to provide common task information to all UEs residing in the cell. When there is a dedicated, active connection, the networks need to send control information,which is done through the Dedicated Control Channel (DCCH). The Dedicated Traffic Channel (DTCH) is used to send dedicated user traffic for one user. Finally, the Common Traffic Channel (CTCH) is used to transmit information either for all users in the cell or for a specific group of users.

For the network to communicate with the UE, all data must be ultimately mapped into the physical channels. From the logical functions over mentioned, and the physical channels, there are the transport channels in between. The information mapping between the three different types of channels is presented in Figure 2.11.
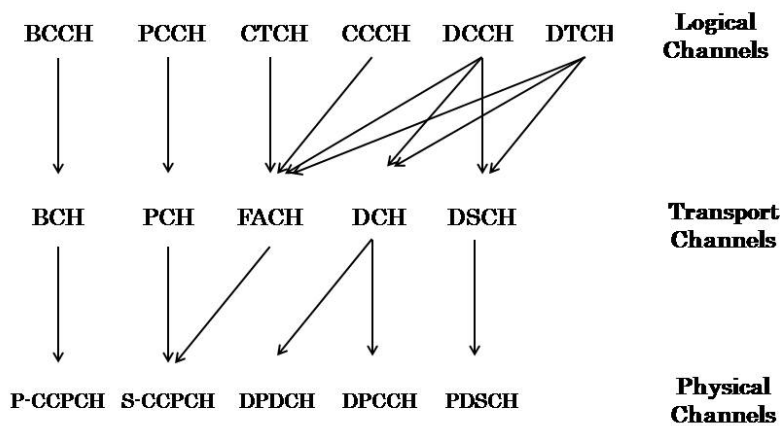
Figure 2.11: UMTS physical channels mapping.

2.4   Long Term Evolution

The 4G and the LTE was materialized from the a disruptive evolution of
the 3G telecommunication systems. The LTE aimed at several system re-
quirements, such as reduced latency, higher user data rates, improved system
capacity/coverage and reduced cost for the operator.

2.4.1   System Architecture

The LTE system architecture consists in Radio Access and CN. The CN is
designated Evolved Packet Core (EPC) and the radio access network is called
Evolved Universal Terrestrial Radio Access Network (E-UTRAN), see Figure
2.12.
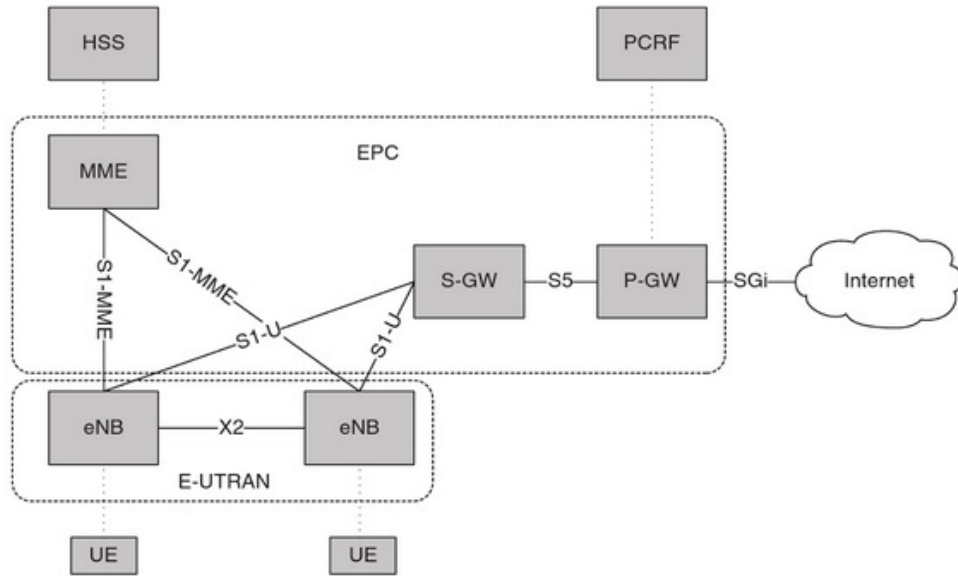
Figure 2.12: LTE system architecture [4].

The E-UTRAN responsibilities fall within either the control-plane or user-
plane support to the UEs. On one hand, the control plane encompasses a
group of protocols for controlling the user data transmission and managing
the connection between the UE and the networks. On the other hand, the
user plane encloses a group of protocols used to support the user data trans-
mission throughout the network. From the UTRAN to the E-UTRAN, the

biggest difference between them, is that an entity responsible for controlling several BS (RNC in the UTRAN), ceased to exist in the E-UTRAN. This was achieved by providing the BS (in LTE system called evolved NodeB (eNB)) with more intelligence.

The EPC is the mobile core network and its responsibilities include mobility management, policy management and security. The EPC is constituted by three entities: Mobility Management Entity (MME), Serving Gateway (S-GW) and Packet Data Network Gateway (P-GW). Compared with previous 3GPP architectures, the EPC has fewer nodes. In part, this is because the LTE system is IP based, eliminating the circuit switch transmission. The end result, addresses one of the major 4G requirements: low latency.

Overall, there are two main interfaces, providing communication between LTE entities, the X2 and S1 interfaces. The interface X2 provides communication among eNB's and can be used to transfer user-plane and control-plane information. The S1 interface connects the eNB to the EPC (either the MME or the S-GW).

2.4.2 Evolved Universal Terrestrial Radio Access Network

The E-UTRAN provides air-interface, user and control plane protocol management for the users. It sustains several functions, for instance, radio resource management, measurements, IP header compression and encryption, broadcast information and others. The only infrastructure in the E-UTRAN is the eNB, as illustrated in Figure 2.13.

Evolved Node B The eNB, on one side, controls all radio interface communication between the UEs. On the other side, it has a direct connection with the MME for control plane communication, and the S-GW for user plane communication. The eNB results from the combination of the 3G BS and the RNC. This step introduced more intelligence in the base station which allowed a more effective resource management. Nonetheless, the removal of a centralized coordination entity as is the RNC has a drawback in the LTE systems. Because it lacks an entity that provides coordination in tasks involving multiple BS. This was overcome, using some complex coordination schemes developed through the exchange of inter-eNB information over the
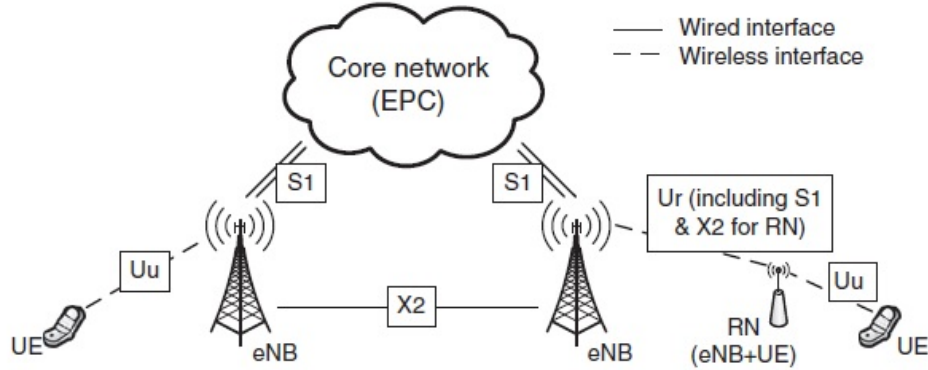
Figure 2.13: EUTRAN architecture [12] .

X2 interface.

The eNB basically includes all functionalities that were previously concentrated in the RNC of the UTRAN system. Moreover, the traditional tasks of the NodeB (NB) are still included in the eNB. So, tasks as RRM, including admission control, radio bearer control, scheduling of user data and control signaling over the air interface are now all concentrated in the eNB.

As the controlling has been moved closer to the radio interface, it reduced the signaling time and amount, reducing the latency for LTE systems.

User Equipment   The user equipment maintained the designation, from 3G networks, of UE and allows the access to the E-UTRAN. It can be either a data modem or a mobile telephone. The UE contains an operator interface for controlling the equipment behavior and a E-UTRAN transceiver. Moreover, it contains a USIM, which provides basic information to identify the mobile subscriber.

2.4.3   Evolved Packet Core

In the previous mobile broadband systems, two separated core networks were needed, one for circuit switched voice applications and another for data switched data applications. For LTE, only a data switched network is needed, as all applications are IP based.

The EPC is constituted by several entities: the MME, the S-GW and

the P-GW. Additionaly two more entities compose the EPC, the Home Subscriber Server (HSS) and the Policy Control and Charging Rules Functions (PCRF) (see Figure 2.12). All these entities that compose the EPC, will provide functions as mobility management, session management, security management, policy control and charging.

The MME is a control entity providing the following functions: bearer management, idle-state mobility handling, user authentication, roaming support, S-GW and P-GW selection and NAS signaling and security. The NAS is a functional layer that provides signaling and traffic between the UE and the P-GW.

The S-GW manages the user data plane between the eNBs and the P-GW. Moreover, the S-GW serves a mobility anchor, ensuring continuous data transmission, as the UE moves across different coverage areas. The S-GW is connected to the eNB through the S1-U interface.

The P-GW provides data connectivity to external packet data networks such as the Internet. Some of the it's functions include packet filtering and routing, and IP address allocation.

The HSS is a database of subscriber related information. It includes information as roaming restrictions, QoS, access-point information, security data, location and service authorization.

The last entity is the PCRF has two main functions: policy control and flow based charging. It defines different charging rules based, for instance, in volume or time of service. Regarding the policy control, it includes gating control, QoS control and usage monitoring functions.

2.4.4 Orthogonal Frequency Division Multiple Access

OFDM divides a wide carrier into numerous narrowband subcarriers, as it can be seen in Figure 2.14. As a radio access system it has been used in different applications such as Wireless LAN standards, cable systems, and many others.

The Orthogonal Frequency-Division Multiple Access (OFDMA), used in LTE air interface, is simply a variant of OFDM, where subcarriers are allocated to different users, transforming the OFDM into a multiple access scheme (see Figure 2.15).

Several key OFDM characteristics are suited to wideband communica-
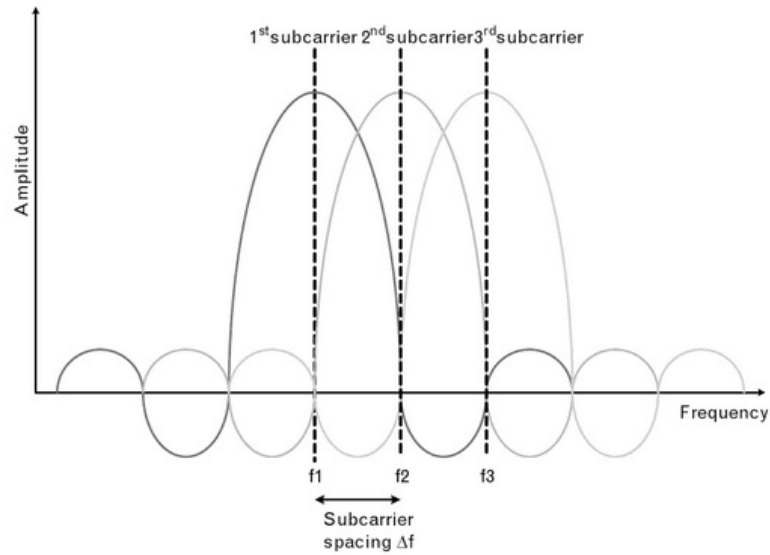
Figure 2.14: Orthogonal frequency division multiplexing [8] .
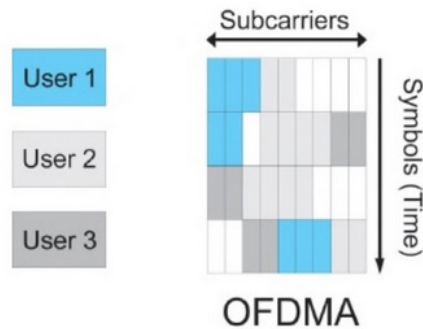
Figure 2.15: Orthogonal frequency division multiple access [17] .

tions. The higher data rates required for 4G networks, are achieved, in part, by the use of wideband carriers. In systems with CDMA or even Time Division Multiple Access (TDMA), the problem with the use of wideband channels, is that such channels, became frequency selective. It could overcome, but a mobile receiver has limited signal processing capacity and power capacity, becoming impractical an implementation of a mobile device capable of dealing with frequency selective channels of bandwidths, like 20 MHz, for instance. The OFDM divides the carrier bandwidth into numerous sub-

carriers, as seen before, being narrow enough for becoming non frequency selective. With such signals, it is much easier to design an efficient mobile receiver.

Normally, with these subcarriers so close together, it would be expected for them to interfere with each other. Nonetheless, the subcarriers frequencies are chosen so that they are orthogonal between each other. In Figure 2.14, when the first carrier reaches its peak amplitude, both the second and third carrier has an amplitude of zero. This behavior turns the subcarriers orthogonal.

As OFDM subcarriers are packed tightly, it makes the OFDM very spectral efficient. Nonetheless, if the frequency synchronization is lost, then the orthogonality between subcarriers is lost, resulting in inter-carrier interference. Another vulnerability of the OFDM is due the radio channel multipath effects. These, may delay some OFDM symbols, which at the receiver, may overlap with other symbols, causing inter-symbol interference.

Chapter 3

Drive Test Reliability

Since the early days DT campaigns to collect RF measurements have been used to provide valuable information in order to assess the performance of wireless networks. Whether it was for propagation model calibration, site validation, troubleshooting or, more recently, for SON, there are still no standards to quantify the quality of a given DT.

This chapter presents a new DT quality assessment model. The model outputs a reliability index, translating the amount and quality of DT data collected for a given cell.

3.1   Drive-Test Data Classification

A DT reliability model was developed to automatically classify the quality
of the DT retrieved data. This model outputs, for a given cell, a reliability
index R based on the quality of the DT data, collected in the cell service
area. On one hand, it encompass the cell's samples geographical distribution
and, on the other hand, the number of collected samples. The reliability
index, R_i, for the ith cell is given by,

$$R_i = \alpha_d D_i + \alpha_s S_i \qquad (3.1)$$

where α_d is the weight of the dispersion index D_i, for cell i and α_s is the
weight of the collected samples ratio S_i, in cell i.

The DT reliability model implementation is presented in Figure 3.1.
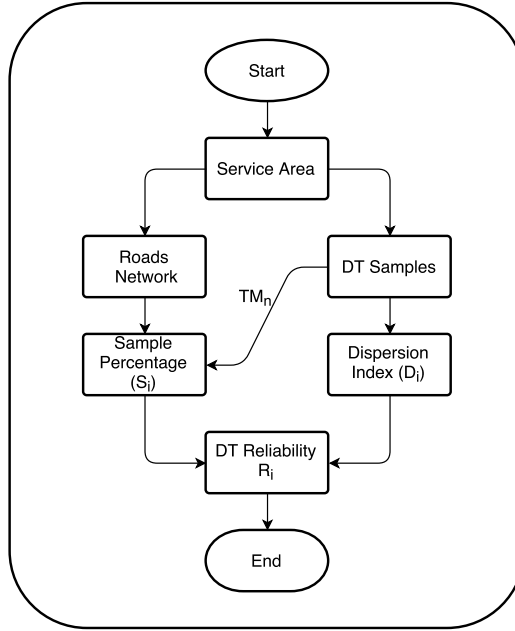
Figure 3.1: DT Reliability flowchart.

It starts with the determination of the cell service area based on the
surrounding topology and radio environment. From now on, the algorithm
retrieves the information needed only for that area. First of all, it identifies all
samples belonging to the cell and that are engaged in the service area. At this
point, the dispersion index D_i is computed. About the sample ratio S_i, road

information in that area must be fetched. It also uses the samples average measurement period (TM_n) to calculated the sample ratio. In the final step, these two indexes are merged and the reliability index R_i is calculated.

3.1.1 Dispersion Index

The quadrant method is a statistical spatial analysis method used in spatial point process models as a mean to test a population point pattern (random, clustered and dispersed) [7]. The spatial point process, is defined as,

$$\{Y(A), A \subseteq P\} \tag{3.2}$$

where P is the study region, A are sub-regions within P and $Y(A)$ is the number of events occurring in area A.

The quadrant method will be used, not as a mean to classify a data set distribution, but as a relative measurement of the dispersion level. The quadrant method or quadrant count method, can be described as the partitioning of the data set into a number of equal sub regions A. These sub regions will be designated as quadrants, typically square areas are utilized. Additionally, other geometrical areas can be used, as long as each of the areas, are equal and do not overlap.

Figure 3.2 presents the used approach, where the blue sector, is the cell which the DT data regards to. All the A areas are delimited with the white color in region P, that is a cell's approximated service area, which is calculated based on the first tier of interference cells.

In each quadrant, the number of occurrences will be counted. Different distributions of the quadrant counts, translate different distributions patterns. This can be influenced by the used quadrant size. On one hand, if a too small quadrant size is chosen, then many quadrants may contain few events, or they may not contain any event at all. On the other hand, a too big quadrant area produces a coarse pattern description. So, a carefully selected quadrant area is highly important, in order to have a good description of the problem under study. Considering,

$$[Y(A_m)]_P = [x_1, ..., x_m] \tag{3.3}$$

where x_m is the number of events in the m quadrant, for all quadrants cover-

Figure 3.2: Cell estimated coverage area.

ing P, the Variance to Mean Ratio (VMR) will be calculated in the following,

$$VRM = \frac{s^2}{\bar{x}} \tag{3.4}$$

where s^2 is the variance of the number of events and $\bar{x}$ the average count number. It measures the data dispersion set in the previous selected study area. The index of dispersion D_i is the normalization of the actual VMR against the worst possible distribution of the ith cell n samples. As so, the index of dispersion D_i is,

$$D_i = \frac{VRM}{VRM_{worst}} \tag{3.5}$$

where VRM_{worst} is calculated using equation 3.4 in the case of all n samples being in one single area A.

3.1.2   Sample Ratio Based on Street Distribution

The DT data used throughout this work has been previously binned. It means that each sample, is the result of an averaging process collected on an area of ten by ten meters. Different DT measurements of the same cell, that

are contained within a bin area, using the average/median or other statistical method, became just one DT measurement to be considered. Hence, on the cell service area it will be replicated the same binning grid with the purpose of comparing the number of DT bins with the theoretical maximum number of bins that could be retrieved in that area, bearing in count the total street extension and the sample rate (TM) of the DT.

The streets information was fetched using an Application Programming Interface (API) from Open Street Map (OSM). It returns the positions of the existing streets within the area of interest. Due to lack of resolution, a linear interpolation was needed, and performed resulting in Figure 3.3.

Figure 3.3: Road/street network.

This interpolation is computed using the same resolution as the DT measurements binning grid, resulting in the maximum samples Max_s that could be collected at a rate r. Regarding the DT sample rate, it varies depending on several variables. The maximum number of RF measurements per second depends on the Radio Access Technology (RAT). Also, the used scanner equipment differs from supplier to supplier and consequently the rates of stored measurements. As the DT may or may not cover different types of roads (e.g., highway, secondary roads), in function of that, the vehicle's speed

will be different. All these factors will result in different average distances between successive samples.

Consider,

$$S = \{a_1, ..., a_n\} \tag{3.6}$$

which is the set of DT samples, with each sample a_n ordered by it's acquisition time, resulting in a chronological set of collected samples. The maximum theoretical number of bins that could be collected must be accounted through the DT sample rate. Hence, to acquire empirically the sample rate, it is performed a DT sample statistical analysis. First of all, it is calculated the Δt_{max} that corresponds to the 50% percentile, Q_2 concerning the difference of time between successive bins,

$$\Delta t_{max} = Q_2 \left(\Delta t_{1,2}, ..., \Delta t_{n-1,n}\right) \tag{3.7}$$

where $\Delta t_{n-1,n}$ is the time delta of capturing two consecutive samples, chronologically. Then, the DT samples average period measurements TM_n for n samples is calculated using the p valid sample pairs below the Δt_{max} limit,

$$TM_n = \frac{\sum \Delta x}{p} \tag{3.8}$$

where Δx is the distance of each p pair.

Finally, merging the information of the total street extension and the previous calculated rate, it produces the maximum samples that the DT could retrieve in that area and in those conditions. At this point, with this maximum number Max_s and the actual number of samples collected, n, the percentage of samples is calculated as it shows,

$$S_i = \frac{n}{Max_s} \frac{r}{TM_n} \tag{3.9}$$

where the second factor, is the correction factor from rate r, which was used to calculate the Max_s samples, to the actual DT sample rate TM_n.

3.2   Model Calibration

At this point, the algorithm allows us to use certain variables to achieve the final DT reliability index for the DT. Using the quadrant method, the service area was split in individual quadrants. Since a typical DT does not

cover all the possible streets and roads within a certain area, a calibration factor should be added. The reliability index encompasses simultaneously the dispersion value of the bins and the percentage of bins collected. Hence, two more variables come into play, the weights of each component. These weights introduce importance into dispersion and road coverage, and its assessment is obliviously dependent on the perception of what is really a well conducted and nicely distributed DT.

3.2.1 Subjective Testing

Subjective testing was achieved by conducting questionnaires to fifty experienced radio engineers that were regularly working with DT data in their radio planning and optimization activities. Thirty DT examples were carefully selected, ranging from empirical bad DT to some quite more extensive DT data. The respondents were asked to classify the DT samples using a quantitative scale from 0 to 10, being 0 very bad and 10 very good. This scale was only used for inquiry practical purposes, as it was then converted to the actual reliability index scale, from 0 to 1. After collecting the data from the questionnaires, the metrics average and the standard deviation were calculated. The calibration was performed through some simulations. The two independent variables (number of areas to divide the study region P and the percentage of road to be considered), were set to a different combination of values. For each combination, the other two variables (the weight of the dispersion index α_d and the weight attributed to the percentage of samples α_s) were adjusted as so the output of the algorithm matches the average value collected from the questionnaires. For each different combinations of tested variables, the indicators presented in Table 3.1, were used as a reference. The $\text{Max}(R)$, $\text{Min}(R)$ and $\text{AVG}(R)$ are the maximum, minimum and

Table 3.1: DT reliability calibration.

	Max(R)	Min(R)	AVG(R)
Inquiry	0.55	0.11	0.32
Algorithm	0.57	0.16	0.33

average value of the R index obtained from the considered DT, respectively.

This calibration process was conducted so that the R_i generated from the algorithm was capable of ranging from the lowest value to the maximum value that resulted from the inquiry. Also the average value from the algorithm for all the DT, should be close to the average from the inquiries.

3.2.2 Model Validation using the Paired Sample T-Test

In order to validate the model, the paired sample T-test was used [2]. It is a statistical technique that compares two population means. It was used to evaluate the existence of correlation between the proposed DT reliability model (R_i) and the the inquiries results. Consider the following setup:

Hypothesis testing   For each of the DT set to inquiry, the produced reliability index was stored as μ_1 and the average value, for the same DT, resulting from the inquiries as μ_2. The thesis is that if this model is valid, the difference D,

$$D = \mu_1 - \mu_2 \tag{3.10}$$

should be zero. As so, the hypothesis test will test the validity of the following conditions:

$$H_0 : \mu_1 - \mu_2 = 0 \tag{3.11}$$

$$H_1 : \mu_1 - \mu_2 \neq 0 \tag{3.12}$$

In order to conduct the test the t parameter is given by,

$$t = \frac{\overline{D}}{\sqrt{\frac{s^2}{n}}} \cap t_{n-1} \tag{3.13}$$

where $\overline{D}$ is the average value of D for all DT, s^2 the variance of D, n the number of DT and using a t-student distribution, t_{n-1}, with $n-1$ freedom degrees.

After the t-parameter being calculated, it is compared with the t-student table value according to the significance level. In this case the results were obtained for a significance level of 5%. If the calculated value is higher than the table value, then we will reject the null hypothesis, H_0, for the paired sample t-test. If the calculated value is lower than the table value, then we

will accept the null hypothesis and assume that there is no significant mean difference between the two paired samples.

Validity of D data   The paired sample t-test assumes that D is normally distributed. To check it the Shapiro-Wilk test for normality [13] was conducted. The values of D were rearranged in ascending order and SQD was calculated as follows,

$$SQD = \sum_{i=1}^{m} (x_i - \overline{x})^2 \tag{3.14}$$

for all m values of D. The second calculated parameter is b and given by,

$$b = \sum_{i=1}^{\frac{m}{2}} \alpha_i (x_{m+1-i} - x_i) \tag{3.15}$$

where the weights α_i are obtained from the Shapiro-Wilk table (based on the value of m). Finally, the statistic test W is,

$$W = \frac{b^2}{SQD} \tag{3.16}$$

Using the test statistics table of Shapiro-Wilks, for m samples, the exact probability of the outcome W, is obtained as *p-value*. This value is compared with a test significance level α (typically 5%),

$$p\text{-}value > \alpha \tag{3.17}$$

where if the *p-value* is higher than α, it can be stated with a $(1 - \alpha)\%$ certainty that the data is normally distributed.

Chapter 4

Low Coverage and High Interference Optimization

As seen, SON algorithms are turning increasingly more important as mobile networks emerge each time more complex in what concerns management and optimization. Hence, self-optimizing algorithms are becoming a valuable asset for competitive mobile operators.

This chapter presents an a description of a self-optimization feature resulted from this research work.

The self-diagnosis algorithms, that identify RF suboptimal scenarios, such as Coverage Holes, Overshooting and Pilot Pollution are presented. These suboptimal situations are detected using DT data and network topology.

Finally, the cell optimization algorithm that proposes new antenna physical parameter configurations, to minimize possible cases of low coverage and high interference is introduced.

4.1   Self-Optimization

Self-Optimization, aims to maintain network quality and performance with a minimum of manual intervention. It monitors and analyses, either Key Performance Indicator (KPI)s, DT measurements, traces[19] or other sources of information, triggering automated actions in the considered network elements.

KPI's are performance indicators which are widely used by mobile operators to assess the network performance. There are KPI's for all sections of a network, since the RAN to the CN. For instance, Call Drop Rate (CDR) or Call Setup Success Rate (CSSR) are two very common RAN KPI's.

Mobile operators have always made extensive DT campaigns to gather RF data. This data is used since a new site is initiated, to assure it's been well deployed, as well with the purpose of optimizing any given area.

By performing a DT campaign, both power and quality of the incoming signals are being continuously measured (might measure different cells signals at the same location and time) and incorporating the Global Positioning System (GPS) locations. This data source provides the support for this work results.

DT data entails considerable operational costs. In alternative, research work has been done to geographically locate an user using the signaling messages exchanged between the terminal equipment and the network. In [19], based on Measurement Report Messages (MRM), a UE was positioned. Moreover, the MRM contains RF measurements, as DT data has. In this way, the algorithms presented in this chapter, can use either DT data or trace based data.

The self-optimization diagram for a network is shown in Figure 4.1. The first block, Data Acquisition, should extract automatically the available performance data, either DT or trace data and network topology. This data should be analyzed by the Self-Diagnosis block, which should detect coverage holes, overshooting and pilot pollution scenarios. If detected, the Optimization block will provide a new antenna configuration to solve or minimize the detected problem. The Operational Support System (OSS) script block is not implemented and remains as future work. It should create the necessary scripts and support files in order to upload the new configurations into the live network.
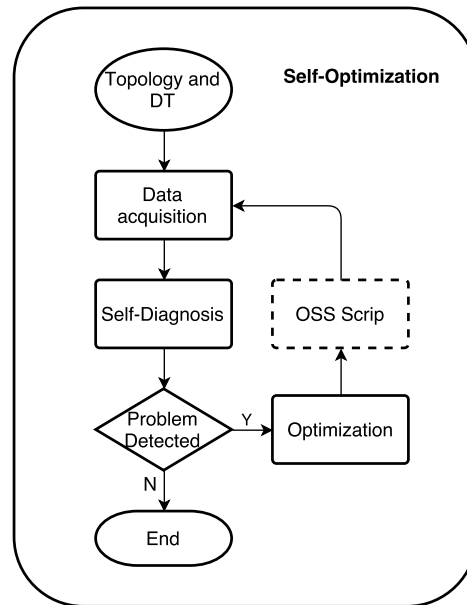
Figure 4.1: SON self-optimization flowchart.

The self-diagnosis module uses either DT measurements or trace data as in Figure 4.2.
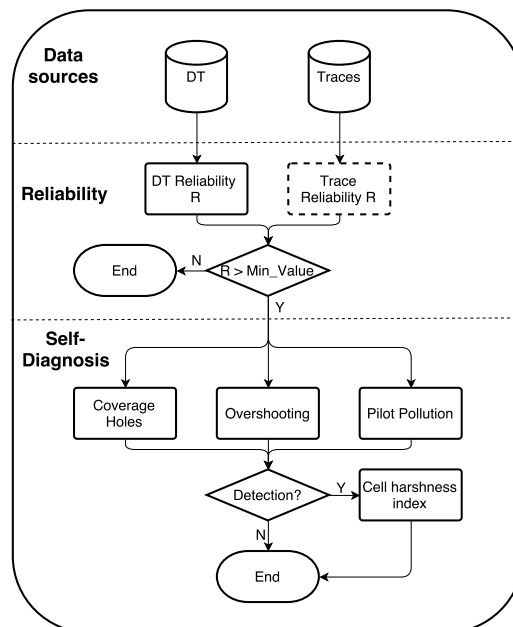
Figure 4.2: Self-diagnosis flowchart.

Thus, with an introduction of a reliability index R for the input data, it accomplishes not only a control mechanism for the self-optimization process, but also increases quality in the self-diagnosis output. Only when the available data, is significant to access the cell's performance, reflected by a value of R higher than a certain threshold, min_value, the self-diagnosis is executed. Otherwise, the available information is not sufficient to retain any strong conclusion.

The self-diagnosis module is composed by three different algorithms, coverage holes, overshooting and pilot pollution, see Figure 4.2. When one of this problems is detected more information is added to the detection result, namely, a harshness index H_{cell} is calculated accessing the problem severity in the cell.

4.2   The Self-Diagnosis Process

The underlying process for the identification of either coverage holes, overshooting or pilot pollution scenarios has a common ground, as presented in Figure 4.3.
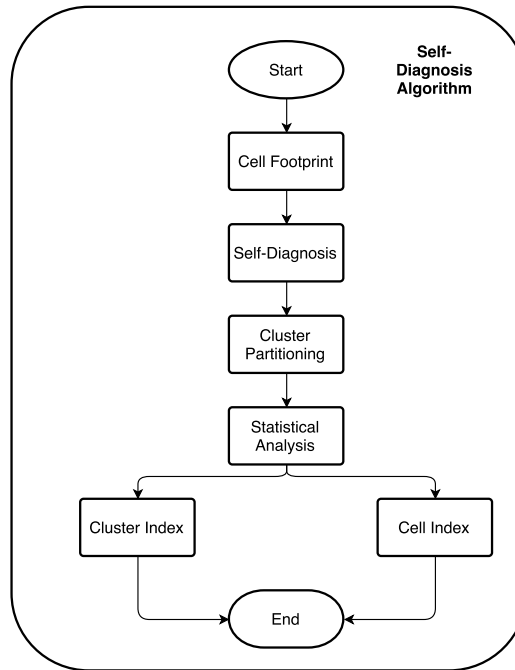
Figure 4.3: General detection flowchart.

The goal is always, regarding the specific algorithm, to diagnose prevalent under performance situations in the form of clusters. Furthermore, to attribute a harshness metric based on a statistical analysis to each cluster, and a harshness level of the cell, including all clusters.

4.2.1 Detecting Coverage Holes

A coverage hole is defined as an area where the pilot (or reference) signal power is in between the lowest network access threshold and the lowest value required for assigning full coverage. Users in this area tend to suffer poor voice or data user experience and possibly dropped calls or high latency.

From the cell's footprint, a coverage hole sample must accomplish two conditions. Firstly, it must be best server or within a small power interval to the best server of the respective bin. To these, we will refer as serving samples. Note that best server is the measurement that corresponds to the best cell, and that should serve the mobiles at that point. Secondly, the best server measurement from the respective serving sample bin, must be below the coverage threshold,

$$BS_{power} < Thr_{CH} \qquad\qquad (4.1)$$

where BS_{power} is the best server value and Thr_{CH} is the minimum serving power value, which is tecnhology (3G/4G) and use case dependent.

Coverage Holes User Inputs The coverage holes self-diagnosis module, as the subsequent self-diagnosis modules, can be used in a self-optimization framework or simply as standalone self-diagnosis module. In the later, it is given to the user some degrees of freedom, in the detection process, in the form of adjustable parameters (See Table 4.1).

The minimum power threshold, sets the network minimum power value admitted. This value typically corresponds to the minimum outdoor design level by service. Below, it is in coverage hole. For 3G it is used the Received Signal Code Power (RSCP) and for 4G it is used the Reference Signal Received Power (RSRP) for the power measurements. The serving RSCP\RSRP Δ, specifies the power range from the best server to be evaluated. The minimum inter-cluster distance, sets the minimum allowed distance between two different clusters. Finally, the last parameter sets the

Table 4.1: Coverage holes detection parameters.

Parameter	Description
Min. Power [dBm]	Minimum coverage threshold.
Serving power Δ [dB]	Coverage delta to the best server.
Min. inter-cluster dist. [m]	Minimum distance between clusters.
Min. bins/cluster [#]	Minimum number of bins per cluster.

minimum number of bins per cluster. These two parameters should be adjusted accordingly to the detection resolution. Moreover, they are common to the foremost self-diagnosis modules, serving the same purpose.

4.2.2 Detecting Overshooting

An overshooting situation occurs when the cells coverage reaches beyond what is planned. Generally, occurs as an "island" of coverage in another cells service area. Overshooted areas may also induce dropped calls and bad quality of experience.

Only the DT measurements, located beyond the cells service area are considered for the overshooting detection. This area, is calculated using the firs tier of the surrounding cells. Then, to be considered overshooting, it must comply with the following conditions, regarding the power value measured,

$$\begin{cases} CSP_{pwr} > Thr_{OS}, & \text{if } CSP \text{ is best} \\ CSP_{pwr} > BS_{pwr} - \Delta_{pwr}, & \text{if } CSP \text{ is not best} \end{cases} \tag{4.2}$$

where CSP_{pwr} is the cell sample power value, Thr_{OS} is the minimum power value to be considered overshooting, BS_{pwr} is the power value of the bin best server cell and Δ_{pwr} is used to define a power range to consider overshooting. Two conditions are presented, for the case when the cell sample, CSP, in analysis is the best server cell and for the opposite case.

Also, the quality of the measurements is evaluated, using the same conditions as Equation 4.2 but regarding the quality measurements,

$$\begin{cases} CSP_{qual} > QThr_{OS}, & \text{if } CSP \text{ is best} \\ CSP_{qual} > BS_{qual} - \Delta_{qual}, & \text{if } CSP \text{ is not best} \end{cases} \tag{4.3}$$

where CSP_{qual} is the cell sample quality value and the $QThr_{OS}$ is the minimum quality threshold. When the cell sample, CSP, is not best server it must be within a quality value range of Δ_{qual} dB's to the best server quality value, BS_{qual}.

Not all overshooting situations are harmful to the network or non-intended. Even though effectively being far from the normal service area, it might happen that, due to terrain profile, it still might be the cell in best condition to serve in that area. In that sense, when the overshooting cells measurements are above the second best server cell by at least a power warning threshold, it indicates the above-mentioned situation. They will still be identified as an overshooting and continue the process, but containing an observation that optimizing this overshooting area might reduce the overall network performance.

Overshooting User Inputs In relation to the adjustable parameters for the overshooting diagnosis, they are presented in Table 4.2. The minimum

Table 4.2: Overshooting detection parameters.

Parameter	Description
Min. power [dBm]	Minimum overshooting power threshold.
Serving power Δ [dB]	Overshooting power delta to the best server.
Min quality [dB]	Minimum overshooting quality threshold.
Serving quality Δ [dB]	Overshooting quality delta to the best server.
Min. inter-cluster dist. [m]	Minimum distance between clusters.
Min. bins/cluster [#]	Minimum number of bins per cluster.

RSCP or RSRP threshold sets the minimum power value, to a DT measurement to be considered overshooting. When a DT is not best server, besides the minimum power threshold, it must be within a serving power delta to the best server. The foremost conditions are also applied to the quality mea-

surements, Energy per chip to Interference Ratio (EcIo)(3G) and Reference Signal Received Quality (RSRQ)(4G).

4.2.3 Detecting Pilot Pollution

Pilot pollution remarks a scenario where too many pilots (or reference signals in the case of LTE) are received in one area. Besides the excess of pilots, it lacks a dominant one. These areas are usually highly interfered, resulting in a poorer user experience.

The DT measurements inducing pilot pollution, are in a serving ranking bellow the ideal maximum number of cells serving in that area. To the cell's footprint where the previous is verified, the following conditions must be complied to be in a pilot pollution situation,

$$\begin{cases} CSP_{pwr} > BS_{pwr} - \Delta_{pwr} \\ CSP_{qual} > BS_{qual} - \Delta_{qual} \end{cases} \tag{4.4}$$

where CSP_{pwr} is the cell sample power value, BS_{pwr} is the power value of the bin best server cell and Δ_{pwr} is used to define a pilot pollution power range. The second condition is equal to the previous, but regarding quality measurements.

Pilot Pollution User Inputs   Considering the pilot pollution self-diagnosis module, the adjustable parameters are displayed in Table 4.3. The minimum power threshold defines a pilot pollution power range.

Both serving deltas (power and quality) set the range of values from the best server to be considered pilot pollution. Finally, the maximum number of serving cells sets the maximum number of cells that, by the network requirements, provide good RF conditions to a single user. Locations where this limit is not complied are eligible for pilot pollution scenarios.

4.2.4 Cluster Partitioning

The radio mobile channel is uncertain due mainly to the effects of fading and multipath. So, the values caught on DT measurements, which are reported at one single instance of time, may not correspond to the average behavior of the radio channel in that point. In order to mitigate this variability,

Table 4.3: Pilot pollution detection parameters.

Parameter	Description
Min. power [dBm]	Minimum pilot pollution power threshold.
Serving power delta [dB]	Pilot pollution power delta to the best server.
Serving quality delta [dB]	Pilot pollution quality delta to the best server.
Max. serving cells [#]	Maximum number of serving cells
Min. inter-cluster dist. [m]	Minimum distance between clusters.
Min. bins/cluster [#]	Minimum number of bins per cluster.

the detection process is executed at the cluster level and not at bin level. This enables to detect prevailing under performance areas and not simply variations, normal and non-correlated with network issues. Therefore, using the auto-correlation distance for shadow fading [9], to limit cluster size, this gives more assertiveness in the detected results.

Regarding the cluster division process itself, it is accomplished using a dendrogram structure [5]. It is a tree diagram that, in this application, translates the distance relation between all DT measurements detected, as in Figure 4.4.
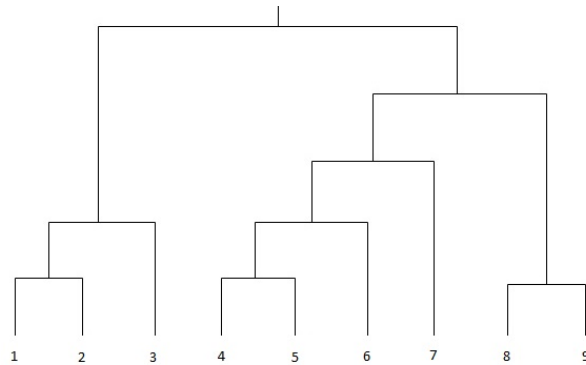
Figure 4.4: Dendrogram structure.

The tree diagram building process, aggregates successively the closest bin/cluster pair until all the bins form a unique cluster. At each aggregation, a different cluster division possibility is built.

The next step is to define which cluster arrangement is the best. Several algorithms accomplish this purpose, and throw different metrics and approaches. Overall what they evaluate is how well concentrated are the points in clusters, when the distance similarity [21] is high. The used approach was the silhouette method [20]. It provides a metric $s(i)$,

$$s_i = \frac{b(i) - a(i)}{max\{a(i), b(i)\}} \tag{4.5}$$

where $a(i)$ is the average dissimilarity to the other points of the cluster, $b(i)$ the lowest average dissimilarity of i to any other cluster. It evaluates how well any given point lies within its cluster. Thus, an $s(i)$ close to one means that the bin is appropriately clustered. This approach is only applied to the cluster division possibilities that respect the maximum cluster size due to the correlation distance.

4.3   Cluster Statistical Analysis

A statistical analysis is conducted to each detected cluster. The purpose is to classify the harshness (severity of the problem) and rank it. The result is a harshness index, $H_{cluster}$, per cluster, given by,

$$H_{cluster} = \frac{\sum_{i=1}^{N} \beta_i U(c(i))}{\sum_{i=1}^{N} \beta_i}, 0 \leq H_{cluster} \leq 1 \tag{4.6}$$

where β_i is the weight for condition i and the $U(c(i))$ is the percentage of bins, from all bins aggregated in one cluster, that verify condition $c(i)$. Once again, these conditions are dependent on the behavior that is being analyzed.

Coverage Holes Statistical Conditions   The coverage hole algorithm calculates it's $H_{cluster}$ index (4.6) using the following conditions,

$$c(i) = Prob(CSP_{power} \leq Thr_i) \quad i \in [1, 3], \tag{4.7}$$

where CSP_{power} is the cell's power measurement value and Thr_i are different coverage thresholds to be compared with. Equation 4.7 is calculated three

times using different thresholds (e.g. $\{-105, -111, -117\}\,dBm$) for a more detailed assessment.

The forth condition is given by,

$$c(4) = Prob(NS_{power} \leq Thr_4) \tag{4.8}$$

where the variable NS_{power} is the power measurement value of the best cell other than the cell being diagnosed and Thr_4 the reference threshold, which has an equal value to the last threshold used in Equation 4.7.

These conditions allow to classify the harshness of a coverage hole in two forms. The condition from Equation (4.7) only concerns to the power value of the source cell. Using different Thr_i values, a cluster will be classified more or less harsh. The forth condition, see Equation (4.8), evaluates the existence of other fallback cell in the cluster. These thresholds are dynamic, defined using as reference the power detection threshold.

The coverage hole harshness index H_{cell} represents a percentage of clusters in coverage hole *vs* the clusters of the cell footprint.This metric might be devious, especially if the DT data is low in number. In that case, the metric will exceed the true percentage value. That's why the DT reliability index R is so important in terms of interpreting the results.

Overshooting Statistical Conditions The overshooting cluster harshness evaluation proceeds with the following conditions,

$$c(i) = Prob(CSP_{power} \geq Thr_i) \quad i \in [1,3], \tag{4.9}$$

where CSP_{power} is the cell's power value and Thr_i are power thresholds to be compared with. Once again, Equation 4.9 is evaluated three times, with different thresholds (e.g. $\{-95, -85, -75\}\,dBm$), allowing more resolution in distinguishing overshooting clusters in severe terms.

The last evaluated condition, aims to quantify the quality degradation caused by the overshooting cell,

$$c(4) = Prob(Degradation_{qual} \geq Thr_{deg}), \tag{4.10}$$

where $Degradation_{qual}$ is calculated based on [15], where an equation was deduced, based on DT data to estimate the quality degradation caused by a given cell. Thr_{deg} is the reference threshold to be compared [15].

The overshooting harshness index H_{cell} represents the average percentage of overshooting clusters against the victim cells footprint, divided also in clusters. Once again, the importance of the DT reliability index must be highlighted.

Pilot Pollution Statistical Conditions   Concerning the pilot pollution algorithm, the conditions to evaluate the harshness level are the following,

$$c(i) = Prob(BS_{qual} \leq Thr_i) \quad i \in [1,3], \tag{4.11}$$

where BS_{qual} is the signal's quality of the best server and Thr_i are the reference values to be compared with (e.g. $\{-10, -14, -18\}\, dB$). The higher the percentage of bins that satisfy Equation 4.11 the more interfered is that area.

Furthermore, the last condition evaluates the best server power values,

$$c(4) = Prob(BS_{power} \leq Thr_4) \tag{4.12}$$

where BS_{power} is the signal power of the best server measurement and Thr_4 is power threshold to serve as reference (e.g. $-90dBm$).

In the pilot pollution case, being a scenario where cells affect another cell performance, the approach for the pilot pollution harshness index H_{cell} is the same as described in the overshooting module.

4.4   Cell Multi-Objective Optimization

Cell coverage optimization and cell interference mitigation, are generally at opposite ends of the cell optimization procedure. For the first, a new set of antenna physical parameters, that increases the cell coverage area, should fix the low coverage issue. To mitigate interference, parameter values that reduce the cell coverage area, are normally preferable. Main point, is that these are conflicting objectives. On achieving one objective, it may lead to miss the other. In such scenarios, a compromise configuration, that minimizes both is proposed.

The inverse configuration for coverage and interference optimization, is partially explained by the fact that a cell is not an isolated system and neither it should be. It should exist a certain amount of overlap between

neighbor cell's coverage areas, to grant user mobility. Nonetheless, if excessive, it generates interference and diminishes the network performance. On the opposite, it might lead to coverage holes between cells and cause high level of drop calls. In fact, coverage and interference optimization, result in the configuration of the antenna physical parameters that harvests the right amount of cell's overlapped areas.

4.4.1 Particle Swarm Optimization

The cell optimization problem is a nonlinear optimization problem. Hence, the need of an optimization algorithm, as is the PSO. The PSO origins are sociologically inspired, considering that the original algorithm was based on the sociological behavior of the bird flocking.

The PSO maintains a population of particles, where each particle constitutes a potential solution to the problem, composing a swarm s. Whereby each particle i, has associated with it, three different characteristics: the current position of the particle x_i, the current speed of the particle v_i and the personal best position of the particle y_i. The personal best position correlated wit a particle is the particle's best position ever yielded (a previous value of x_i). In a minimization problem, as is the cell multi-objective optimization, the smaller function value is, the higher fitness it has. The objective function that is being minimized is denoted by the symbol f. Being an iterative algorithm, at each iteration, the personal best position is updated according to Equation 4.13, with dependence on the time step t.

$$y_i(t+1) = \begin{cases} y_i(t) & \text{if} \quad f(x_i(t+1) \geq f(y_i(t) \\ x_i(t+1) & \text{if} \quad f(x_i(t+1) < f(y_i(t) \end{cases} \qquad (4.13)$$

It was used the PSO *gbest* model instead of the PSO *lbest* model due to it's faster rate of convergence. This model maintains a single best solution $\hat{y}$, which is the best position discovered by any of the particles until the instant t.

In Figure 4.5 the position and speed vector of all particles x_i composing a swarm s in two different iterations are presented. The optimal solution is $(x_1, x_2) = (0, 0)$ and the red dot at each time instance is the global best position $\hat{y}$. When time $t = 0$ the swarm particles are considerably dispersed but tending to converge to the $\hat{y}$ position. Meanwhile, the next iteration,
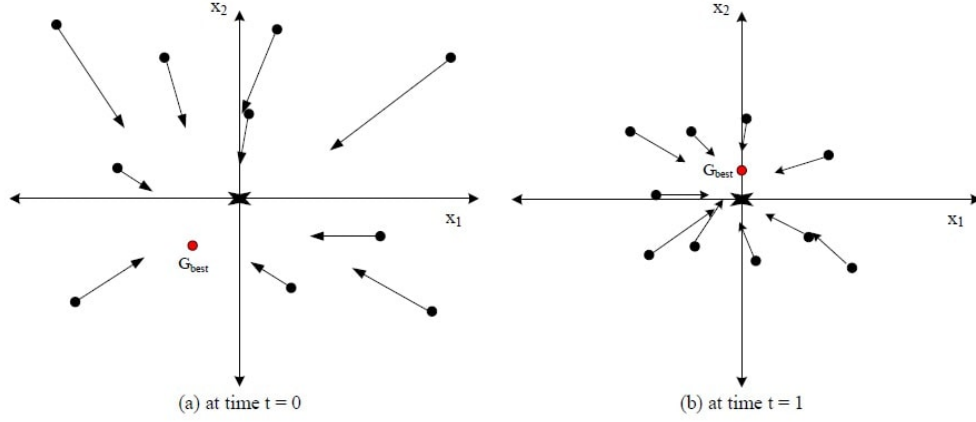
(a) at time t = 0   (b) at time t = 1

Figure 4.5: Speed and position updated for multi-particle in gbest PSO [16].

attempts to reach the previous global best position discovering a new $\hat{y}$. The latest $\hat{y}$ position is closer to the optimal solution and the swarm is converging for the new global best position. A few more iterations and eventually the swarm will converge to the optimal solution.

In turn, the particle speed is calculated, at each algorithm iteration. It makes use of two independent random sequences $r_1 \sim U(0,1)$ and $r_1 \sim U(0,1)$, providing the stochastic nature of the algorithm. Furthermore, the values r_1 and r_2 are scaled by two constants $0 < c_1, c_2 \leq 2$. These constants are called acceleration coefficients and they control the maximum speed step that a particle can take in a single iteration (see Equation 4.14). The last constant w is called inertia weight and it controls how much of the previous speed should be retained from the previous time step. The particle speed is specified separately for each dimension $j \in 1..n$, so that $v_{i,j}$ stands for the jth dimension of the speed vector associated with the i_{th} particle, as shown in:

$$v_{i,j}(t+1) = wv_{i,j}(t) + c_1 r_{1,j}(t)[y_{i,j}(t) - x_{i,j}(t)] + c_2 r_{2,j}(t)[\hat{y}_j(t) - x_{i,j}(t)]. \quad (4.14)$$

From the speed update equation, it can be asserted that c_1 defines the maximum step size towards the personal best position of that particle and c_2 sets the maximum step size in the direction of the global best particle.

The speed value is governed by three terms. The first, $v_{i,j}(t)$, is an in-

ertial component, which contributes to the exploratory characteristic of the algorithm. The bottom line, is that the algorithm particles, in a first stage, should explore the solution space, and in a second stage, converge to an optimal solution. The inertia values in the beginning tend to be high as all particles are disperse. In the later stage, as the particle, start to converge to the optimal solution, its velocity is smaller as well as the inertia value. In addition, it is scaled by the factor w. This was one of the earliest modifications to the original PSO algorithm, aimed at improving the rate of convergence. According to [14], choosing $w \in [0.8, 1.2]$ results in faster convergence. The second component $c_1 r_{1,j}(t)[y_{i,j}(t) - x_{i,j}(t)]$ is associated with the cognition, considering that it only takes into account the particle's own experiences.

The third term is $c_2 r_{2,j}(t)[\hat{y}_j(t) - x_{i,j}(t)]$ which represents the social iteration between particles. The global best position $\hat{y}$ acts as an attractor, pulling all the particles towards it. Sooner or later, all the particles will converge to this position, that should be the optimal solution.

These three components are presented in Figure 4.6. It can be seen the particle initial position x_i and the different speed components (inertia, cognitive and social) that contributed for the new particle position. Looking
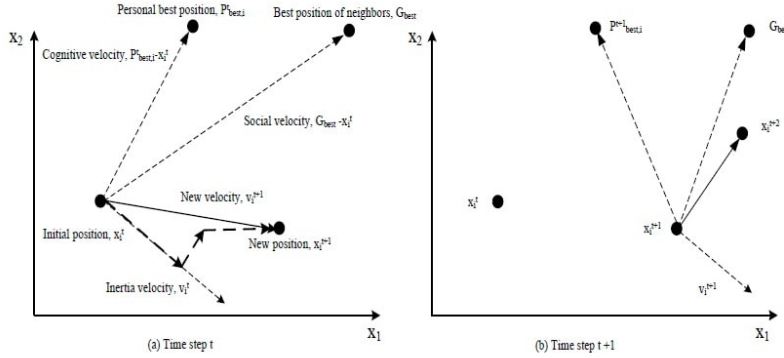

Figure 4.6: Speed and position updated for a particle [16].

at the particle position at the two time instants it can be asserted that the particle is converging to the global best position found by any particle of the swarm.

About the algorithm convergence, in [18] was generalized an equation that specifies the magnitude relation between each of the speed update constants

$(w$, c_1 and $c_2)$, which is given by,

$$w > \frac{1}{2}(c_1 + c_2) - 1 \tag{4.15}$$

When choosing values that complies with the Equation 4.15, it assures that the algorithm converges to a solution, nevertheless, it does not guarantee that it will be the optimal solution. Depending on the objective function, some times it may converge to local minimum instead of the global minimum.

The position of each particle is updated using the new speed vector (Equation 4.14) so that,

$$x_i(t + 1) = x_i(t) + v_i(t + 1) \tag{4.16}$$

The Algorithm 1 specifies a generic PSO algorithm, and it consists in a repeated application of the update equations presented above. It requires an initialization aimed to setup each coordinate $x_{i,j}$ to a value drawn from the uniform distribution on the interval $[-x_{max}, x_{max}]$, for all $i \in 1..s$ and $j \in 1..n$. This assigns the initial particles positions throughout the search space. Then, each $v_{i,j}$ is initialized with a value from the interval $[-v_{max}, v_{max}]$, for all $i \in 1..s$ and $j \in 1..n$. Alternately, it can be initialized with 0, as the initial positions are already randomized.

Algorithm 1 Pseudo code for the original PSO algorithm

1: Initialize an n-dimensional PSO: S
2:
3: **while** $stopping condition is false$ **do**
4:     **for** each particle $i \in [1..s]$ **do**
5:         **if** $f(S.x_i) < f(S.x_i)$ **then**
6:             $S.y_i = S.x_i$
7:         **if** $f(S.y_i) < f(S.\hat{y})$ **then**
8:             $S.\hat{y} = S.y_i$
9:         PSO updates using Equations (4.14-4.16)

Finally, the algorithm is executed until the stopping criteria is fulfilled. Concerning, the stopping criteria, there are several. The most common one is to execute the algorithm until a fixed number of iterations. However, others such as checking that all particles stopped (set Equation 4.14 equal to zero) is also a valid stopping criteria.

The algorithm works as follows: initially, one particle is identified as the best particle due to its fitness value. Then, all the other particles are accelerated towards it, but also in the direction of their best solutions that they have been discovering previously. Occasionally, the particles will overshoot their target and consequently explore the search space surrounding the currently best particles. Since most objective functions have some continuity, the probability of having a good solution surrounded by equally good, or better solutions, is high. By approaching the currently best solution from several directions, changes are good, since these neighboring solutions will be discovered by one of the swarm particles.

4.4.2 Optimization Targets

The cell optimization process aims to minimize coverage holes, overshooting and pilot pollution scenarios. Thus, the PSO algorithm minimizes an objective function, which is the result of a linear combination of objective functions for each optimization target, that is in between the range, $C(\Omega) \in [0, 1]$ and is given by Equation 4.17,

$$C(\Omega) = \alpha_1 C_{CH(\Omega)} + \alpha_2 C_{OS(\Omega)} + \alpha_3 C_{PP(\Omega)}, \qquad (4.17)$$

where Ω represents the set of antenna adjustable parameter values, and C_{CH}, C_{OS}, C_{PP} are the objective function for coverage holes, overshooting and pilot pollution targets, respectively. The α_1, α_2 and α_3 are the respective optimization weights of the given targets, provided that the rule $\alpha_1 + \alpha_2 + \alpha_3 = 1$ is fulfilled. Furthermore, by being adjustable, it allows to adjust the cell optimization algorithm to particular use cases. In the case where a solution that solves the three problems, is unfeasible, any of the optimization targets might be of more priority, which could be denoted by a greater weight.

In turn, an optimization target objective function provides values in the range $C_{target}(\Omega) \in [0, 1]$ and is calculated using Equation 4.18,

$$C_{target}(\Omega) = \beta_1 \sum_{c=1}^{k} \left(\frac{c_{bins}}{B} \times H_{cluster} \right) + \beta_2 \frac{k}{T}, \qquad (4.18)$$

where k is the number of clusters with the target issue, c_{bins} is the number of bins in the cluster c, B is the total number of the target clusters bins, $H_{cluster}$

is the target cluster severity level and T is the total number of clusters that compose the cells footprint. β_1 and β_2 are configurable, in order to optimize based on the number of the detected data or it's severity for the network.

The $H_{cluster}$ indicates the harshness of a cluster in terms of any optimization target, and calculated as is described in Section 4.3.

Reflecting the concern of diminishing the neighbor cells performance by optimizing one cell, and the fact that it was common to identify multiple antenna configurations that minimize to zero the objective function, a secondary objective function, $M(\Omega)$, was added. It aimed to provide a single solution to any cell optimization scenario and to minimize performance degradation in the neighbor cells. This secondary function is only minimized if the primary objective function is totally minimized ($C(\Omega) = 0$) as is illustrated in Figure 4.7.
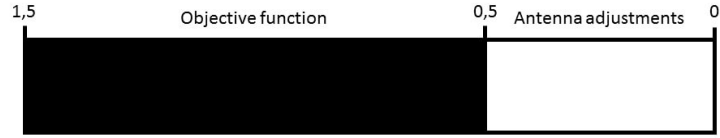
Figure 4.7: Primary and secondary objective function.

The bottom line is that the cell optimization algorithm should minimize the objective targets and return an antenna configuration that is as closest as possible to the original antenna configuration. This condition is evaluated by $M(\Omega)$ and it corresponds to the white range of values in Figure 4.7. In fact, Figure 4.7 represents the new global objective function given by,

$$G(\Omega) = C(\Omega) + M(\Omega) + 0.5, \tag{4.19}$$

where $M(\Omega)$ is given by,

$$M(\Omega) = \begin{cases} -\left(0.5 - \frac{\sum_{p=1}^{j}(|\Omega_p - A_j|)}{2\sum_{p=1}^{j}(\Delta_j)}\right) & C(\Omega) = 0 \\ 0 & C(\Omega) > 0 \end{cases}, \tag{4.20}$$

where j is an antenna adjustable parameter value, from the actual configuration Ω, A_j is the original antenna parameter value and Δ_j is the maximum

value difference, from the antenna original configuration, that a new configuration can obtain. Note that $M(\Omega) \in [-0.5, 0]$ where -0.5 represents a configuration equal to the original configuration. The key point is that it acts as a similarity measurement to the original antenna configuration, and a new configuration will be preferred as much as the similarity to the original configuration.

4.4.3   Cell Optimization Algorithm

The cell optimization algorithm can optimize the cells physical parameters in order to optimize any or all of the possible optimization targets: coverage holes, overshooting and pilot pollution, see Figure 4.8.
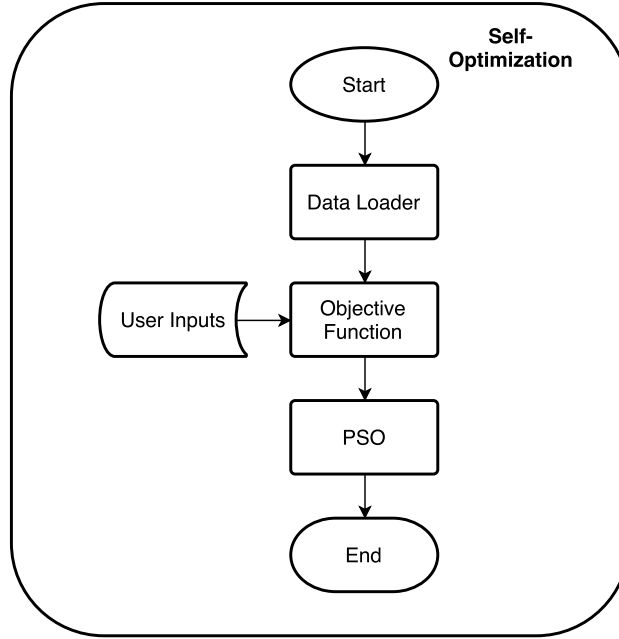
Figure 4.8: Antenna optimization algorithm.

The adjustable antenna physical parameters are the Mechanical Downtilt (MDT), Electrical Downtilt (EDT) and the antenna orientation, being all optional.The first block is the data loader. The responsibility of this loader is to retrieve all DT data relevant for the cell being optimized. Hence, it gathers from a database the cell complete footprint. The fetched bins are then divided into clusters in order to apply the $H_{cluster}$ (Equation 4.6) used in the PSO objective functions.

Moreover, there are two criteria, applied to each cluster, that sets which possible optimization target it should be evaluated for (see Table 4.4). Consequently clusters located beyond the overshooting area (as defined in Subsection 4.2.2) will be evaluated for overshooting issues. If in the cluster area, the cell being optimized is dominant or co-dominant, it will be evaluated for coverage holes. In case the cell being optimized is non dominant, in a cluster, pilot pollution is appraised.

Table 4.4: Cluster optimization target criteria.

Coverage Holes Clusters	Overshooting Clusters	Pilot Pollution clusters
Source is dominant or co-dominant	Outside overshooting area	Source is non dominant

The user can customize some parameters of the objective function, the antenna physical parameters that should be optimized as well as some properties of PSO algorithm (See Table 4.5). The cell optimization algorithm can optimize any or all the three optimization targets. Besides, two new options allow to, in consequence of a new antenna configuration, to control if the cell service area could or not increase/decrease. The decrease option is only applied to clusters where there is lack of cell dominance. Clusters where the cell being optimized is dominant are secured.

Regarding the PSO algorithm two variables are user configurable. The maximum number of iterations should be chosen, bearing in mind that with a higher number, the probability of convergence of the algorithm to a solution is greater, but at the expenditure of delayed processing time. The number of initial particles results also from a trade-off between time and convergence probability.

The final processing block, it is the optimization itself. The PSO algorithm will generate new possible antenna configurations and evaluate them using the objective function (Equation 4.19).

The adjustment of any of the antenna parameters above-mentioned, will lead to an antenna gain variation. For a given location, a variation of gain in the transmitter, results in the same variation in terms of received power,

Table 4.5: Cell optimization parameters.

	Parameter	Description
Antenna	MDT*	Optimize mechanical tilt
	EDT*	Optimize electrical tilt
	Orientation*	Optimize orientation
Optimization targets	Coverage Holes*	Optimize coverage holes
	Overshooting*	Optimize overshooting
	Pilot Pollution*	Optimize pilot pollution
	Increase service area	Allow a configuration that increases the service area
	Decrease service area	Allow a configuration that decreases the service area
PSO algorithm	Max iterations	Maximum number of iterations
	Initial particles	Number of the PSO particles

*Optional parameters.

as in Equation 4.21,

$$P_r = P_t - L_t + G_t - L_{Path} + G_r, \tag{4.21}$$

where P_r is the received power, P_t is the transmitter power, L_t is the transmitter power losses, G_t is the transmitter antenna gain, L_{Path} is the path loss and G_r is the receiver antenna gain. As a new antenna configuration only affects the transmitter antenna gain, G_t, and all the others terms of Equation 4.21 remain constant, it is estimated the RSCP and RSRP values that would be received by a terminal equipment.

Regarding, the antenna gain variation, it can be estimated either through a theoretical antenna radiation pattern model [1] or using the real antenna pattern. In this work, the theoretical 3GPP model was considered.

Overall, each PSO particle position identifies a different antenna configuration. In order to evaluate the fitness of the solution, all the samples of the cell footprint are updated with the new correspondent power values, due to the different transmitter gain. Then each cluster is evaluated in terms of coverage holes, overshooting and pilot pollution. In consequence, the global objective function translates for all footprint clusters the presence and magnitude of any of the above-mentioned RF issues. In this way, the algorithm achieves a configuration that minimizes the initial problems without causing

new RF performance issues in other clusters that initially had no performance issues.

Chapter 5

Results

In this chapter it is presented the DT reliability index model calibration allied with the final results of the algorithm. It includes several case study scenarios, for different types of environments (urban, suburban and rural) and also several degrees of quality concerning the DT execution.

Concerning the self-diagnosis modules (coverage holes, overshooting and pilot pollution), these were tested for 3G and 4G cells in urban, suburban and rural scenarios. A handful of cells are presented with the above-mentioned issues.

For the antenna self-optimization algorithm some examples are presented where the algorithm identified a new antenna configuration that solved or minimized the cell performance maters.

It is important to note that that both the DT data and the network topology information were real data from a mobile network operator.

5.1   Drive Test Reliability Index

In this section the results concerning the DT quality classification in the form of the DT reliability index R are presented. It includes the model calibration results mentioned in Section 3.2 and the final reliability index R results.

Model Calibration   The inquiry contained DT examples for urban, suburban and rural environments. As the typical cell service area radius is different, within these case scenarios, as also the street extension and it's arrangement, the model was calibrated individually to each radio environment.

The results of the calibration process are presented in Table 5.1. As seen,

Table 5.1: DT model calibration result.

	Urban	Suburban	Rural
Number of Areas	36	36	36
Street Percentage	80%	80%	80%
Samples Ratio Factor (α_s)	71%	69%	55%
Dispersion Factor (α_d)	29%	31%	45%

using the quadrant method [7], the cell service area can be divided in any number of smaller areas, as long as all have the same area size. So, the number of areas (Table 5.1) sets the number of areas for the cell service area. Note that the dispersion index D_i is dependent of the number of areas. For the same data set of cell samples, on calculating the dispersion index, with different number of areas would result in different dispersion values.

The average DT does not cover 100% of the road/street network within a cell service area. Consequently, it was unrealistic for the model to expect a 100% street coverage. Moreover, by applying a street percentage factor (see Table 5.1), where the model considers that covering at least a given percentage of the total street network is optimal, it provides more resolution to the DT reliability index (R). Once again, but in relation to the collected samples ratio S_i, it is dependent of the considered street percentage. Regarding the dispersion (α_d) and the samples ratio (α_s) factors, these are used to calibrate the weights of the dispersion index and the collected samples ratio (Equation 3.1).

In fact, the DT quality evaluation differs from one radio environment to another. It can be ascertained that when the cell service area increases, the dispersion of the samples presents more relevance comparing to the smaller cell service areas (urban). The bottom line is for dense urban environments, the number of collected bins gains importance. In the opposite, for rural, with larger services areas and less density of streets and roads, the dispersion of samples becomes almost as important as the sheer number of it.

After the algorithm implementation and parameterization, the paired t-test was performed to assure the validity of the algorithm's R_i indexes for the three case scenarios (see Table 5.2).

Table 5.2: DT Paired sample t-test result.

Environment	$\mu(D)$	$\sigma(D)$	Test value	t-student
Urban	-0.0004	0.0453	-0.0318	1.7960
Suburban	-0.0035	0.0540	-0.1450	2.1320
Rural	-0.0150	0.0814	-0.3191	2.9200

As stated, the null hypothesis, $H_0 : \mu_1 - \mu_2 = 0$, was tested for a significance level of 5% and it was assured that the values of D followed a normal distribution using the Shapiro-Wilks test for normality. As the test values are within the limits of retaining the null hypothesis, within the t-student and his symmetric, the null hypothesis was accepted, with a 95% confidence interval. This assures that there is statistical support that no significant difference, between the R_i indexes from the algorithm and the inquire indexes, is evidenced, which validates the algorithm using the professional experience of fifty radio experts in this field of work.

Reliability Index The algorithm was tested for urban, suburban and rural environments for a wide range of DT data. In the following, some visual examples will be presented, along with the model outcome, which is the reliability index.

In Figure 5.1 the proposed model indicates a low reliability index R of 0.14 due to the lack of collected samples. Visually, it can be observed that the available data, in respect to the blue cell, is very diminutive in terms of collect measurements. In the same way, it can seen that the road network allowed the DT to collect more data.
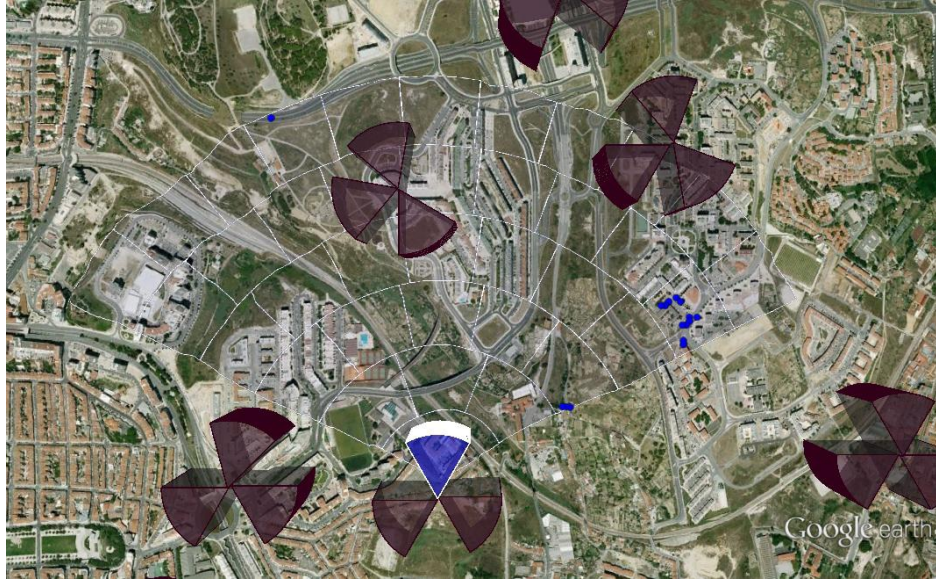
Figure 5.1: DT with low reliability.

In Figure 5.2, the DT data increases in number and in dispersion, enhancing the reliability index R value to $0, 46$.
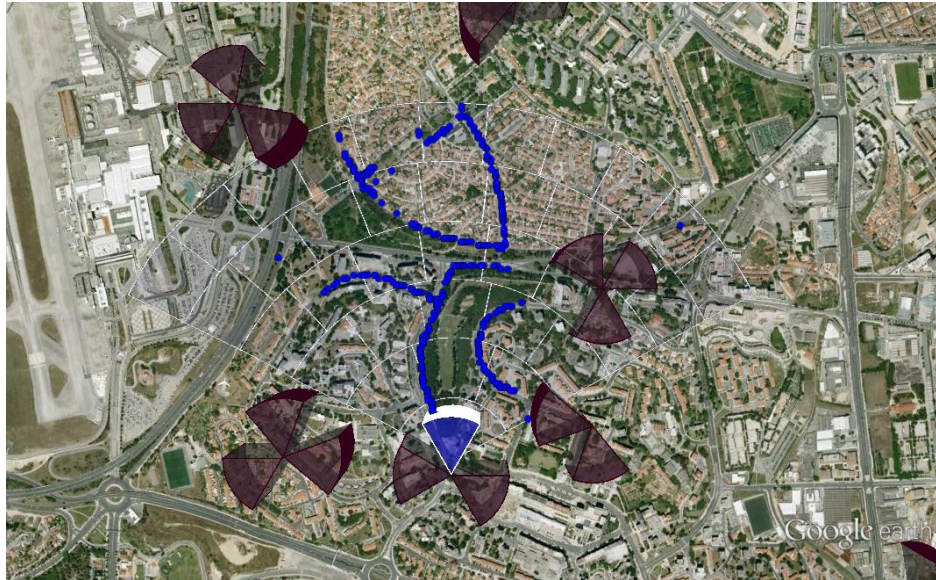

Figure 5.2: DT with medium reliability.

The number of collected measurements and its dispersion are more significant than the previous example. Nonetheless, a significant road extension

was not covered by the DT, hence a reliability value of 0.46.

The last example, in Figure 5.3, the DT covers a good percentage of streets available and with a good dispersion of samples, which boosts the reliability index to 0.73. Even though, a significant part of the analyzed area

Figure 5.3: DT with high reliability.

does not contain DT data, as these areas are disproved of a road network, they are not taken into account.

Finally, it is important to note that the proposed algorithm, by introducing automatic classification of DT based in subjective inquiries allows the knowledge transfer from the radio experts to the automatic optimization algorithms under development, enabling that the optimized network settings are achieved based on reliable DT measurements.

5.2   Self-Diagnosis Modules

The self-diagnosis algorithms were tested for both technologies (UMTS and LTE) in different radio propagation environments, urban, suburban and rural. In order to concise the results it was decided to firstly present a more comprehensive analysis of an urban area in regard to the UMTS cells. Secondly, to complement the overall results of this work, some individual exam-

ples of LTE cells in rural environments are also presented.

The coverage holes, overshooting and pilot pollution algorithms were applied in a live network, and for an urban scenario. 830 3G cells operating at different frequencies were self-diagnosed, and performance metrics were computed. Extensive DT data corresponding to this area was used.

The set of parameters, for coverage holes (CH), overshooting (OS) and pilot pollution (PP) are detailed in Table 5.3.

Table 5.3: Self-diagnosis detection parameters.

	CH	OS	PP
RSCP threshold [dBm]	-100	-95	-95
RSCP delta [dB]	3	6	6
Min Ec/N0 threshold [dB]	N/A	-10	N/A
Ec/N0 delta [dB]	N/A	6	4
Bins/Cluster [#]	10	10	10
Min inter-cluster distance [m]	57.5	57.5	57.5
Max serving cells	N/A	N/A	3

These used thresholds to identify the intended network behaviors (section 4.2), are extremely dependent on mobile operator policies, requirements, type of service, etc., so a set of default parameters values was used.

The results of the diagnosis for the urban area are shown in Table 5.4 and in Figure 5.4. The columns "CH","OS" and "PP" refer to coverage holes, overshooting and pilot pollution algorithms, respectively. Moreover, this results were obtained from analyzing 830 different cells.

Table 5.4: Self-diagnosis detected scenarios.

	CH	OS	PP
Detected cells	13	35	64
Average clusters [#]	3	2	3
Average index H_{cell}	38	11	11
Average index R	37	45	55

The results in Table 5.4, reveal a considerable number of cells with performance malfunctions, where the number of cells with interference problems is significantly higher than coverage issues.
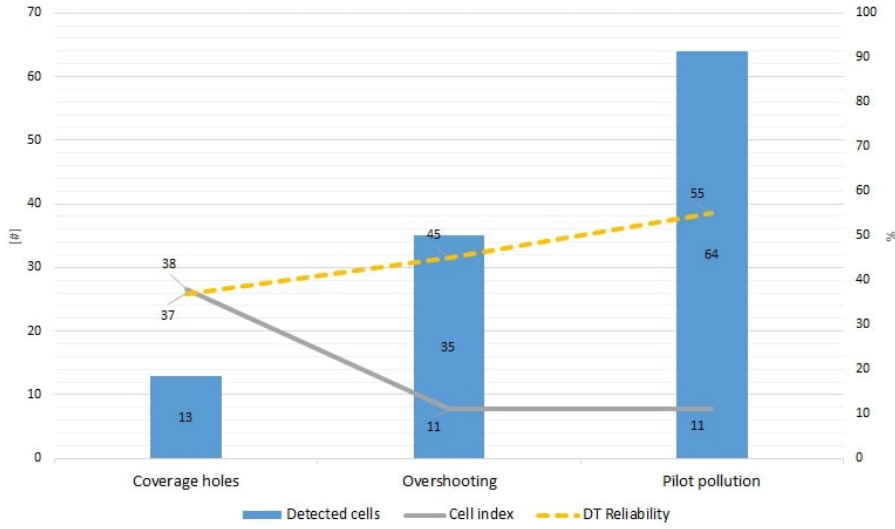
Figure 5.4: Self-diagnosis overview results.

Based on Figure 5.4, it can be ascertained that, in regard to the average H_{cell} values, the coverage holes algorithm exhibits the highest. The coverage holes DT reliability index R is the lowest, though. Which sets that the DT did not retrieve data from all cell service area, leading to an overestimated H_{cell} value.

With regard to the interference detection algorithms, the average cell index H_{cell} was 11% with more quality of the respective DT data.

5.2.1 UMTS - Coverage Holes

One of the detected coverage holes is illustrated in Figure 5.5.

It corresponds to an urban scenario environment, where the blue cell is the diagnosed cell, with the red points corresponding to the cell's measurements in coverage hole, grouped in one cluster. In this cluster area, the source cell is the only dominant cell. The cell represented over the coverage hole cluster corresponds to an indoor cell, which does not contributed to outdoor coverage.

Concerning the DT data itself, in coverage hole, it was detected 14 bins. They are at 800 meters from the diagnosed cell, with an average RSCP value of -104 dBm, which is below the coverage threshold.

The elevation profiling and the 3D building modulation of this example,
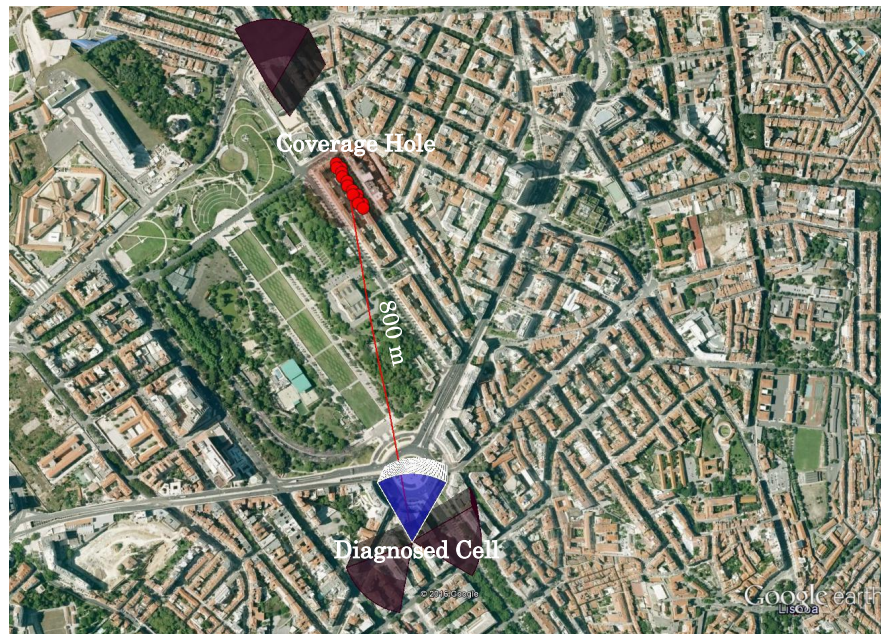
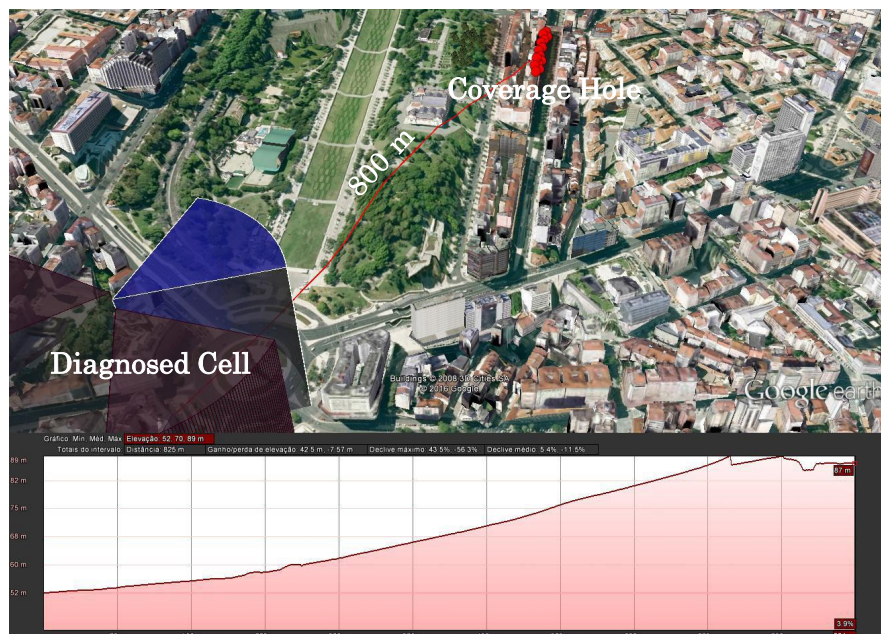Figure 5.5: UMTS - coverage hole scenario.

can be seen in Figure 5.6.

Figure 5.6: UMTS - coverage hole cluster terrain profile.

It can be asserted that the coverage hole area is in NLoS, due to building obstruction and terrain elevation. In addiction, the cell is parameterized with downtilt, that decreases the cells service area.

In relation to the index H_{cell}, for this occurrence, it was 25%, meaning that 25% of the clusters are in coverage hole. Nevertheless, as the DT reliability index R for the cell was only 23%, it indicates that the index H_{cell} can be off the real percentage.

5.2.2 UMTS - Overshooting

Concerning the overshooting, Figure 5.7 illustrates an overshooting in an overlap area between two cells.
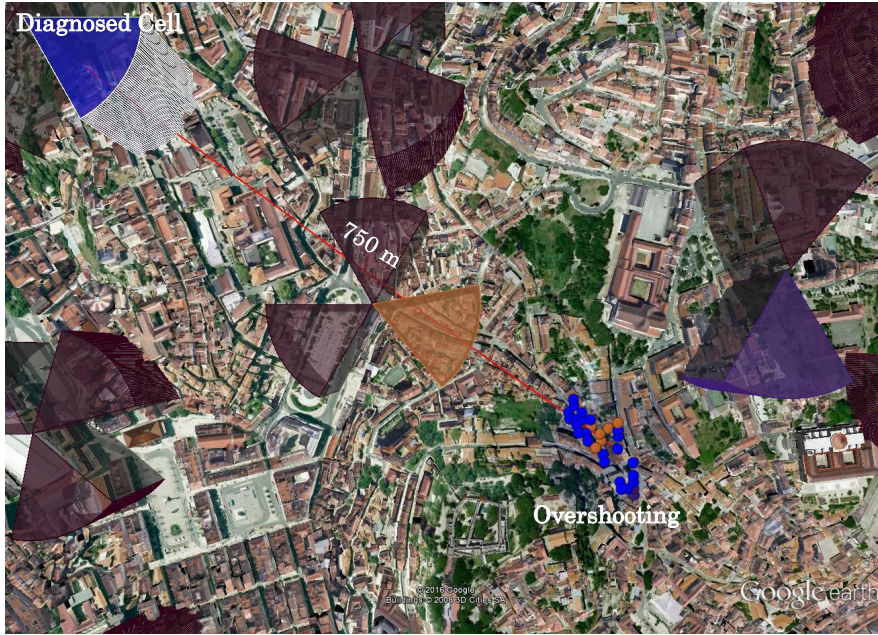

Figure 5.7: UMTS - overshooting scenario.

Again, the blue cell is the diagnosed cell, and in this case, it was detected one overshooting cluster, at 750 meters of distance. The detected overshooting samples have an average RSCP value of -69 dBm and an average value of EcIo of -9 dB. In addition, the cells with orange and purple colors, were identified as the victim cells, in the sense that, the overshooting cluster is located in their service areas. The blue cell is reaching the other two cell's service areas with a high power, causing interference.

Just for additional information, see Figure 5.8, where the terrain profile between the source cell and the respective overshooting cluster is illustrated.
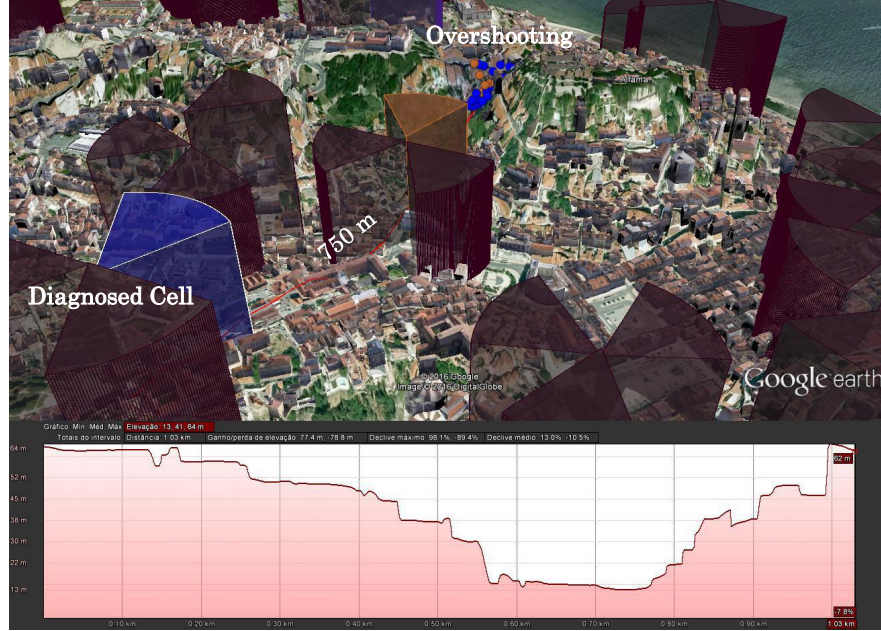

Figure 5.8: UMTS - overshooting cluster terrain profile.

It exists LoS between the source cell and the overshooting cluster, which enables the overshooting scenario.

In regard to the overshooting cell index, H_{cell}, it was obtained a value of 9%. This represents, in this particular case, that the overshooting clusters affected, on average, 9% of the victim cells footprint. Concerning the DT reliability index R, it was obtained an average value of 41% for the two victim cells.

5.2.3   UMTS - Pilot Pollution

Regarding the pilot pollution detection algorithm, an example is illustrated in Figure 5.9. The diagnosed cell (in blue) is reaching an area, within the pilot pollution conditions (4.2.3), where the highlighted cells are the best serving for each respective bin. The detected pilot pollution bins, were grouped in two valid clusters. Even though, the cell samples are ranked above the maximum number of serving cells, they exhibit an average RSCP value of -72 dBm and an average EcIo of -17 dB. Even for the high average power

Figure 5.9: UMTS - pilot pollution scenario.

detected, the average quality level is very low, stressing how interfered is this area.

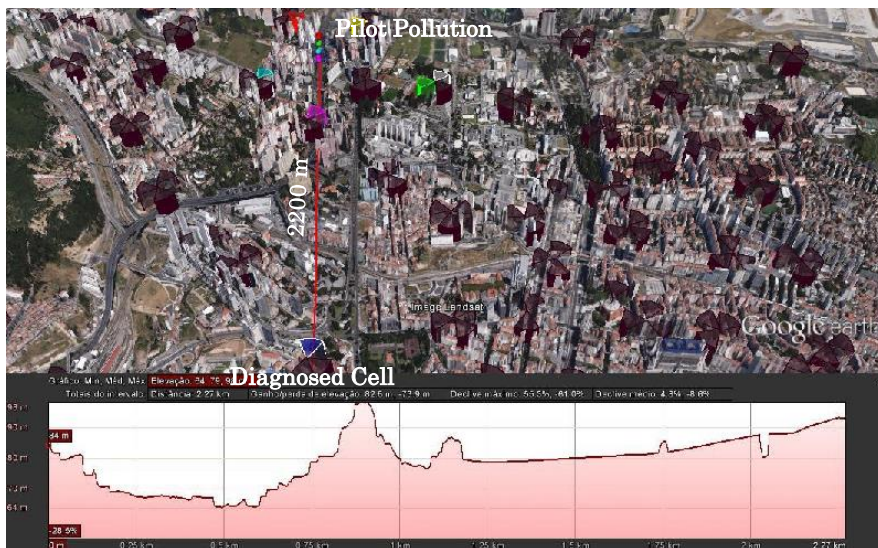Figure 5.10 presents the height profile between the diagnosed cell and detected clusters.

Figure 5.10: UMTS - Pilot pollution cluster terrain profile.

Taking into account the antenna height, it is almost an LoS scenario,

which associated with the lack of the cell downtilt enables this interference scenario. Moreover, as this cell operates in the 900 MHz band, the received power is high, for the distance of 2 km between the blue cell and the pilot pollution clusters.

By definition, pilot pollution areas display an excessive number of pilot signals. Sometimes, this number is high enough, that enables the algorithm to suggest which cell(s) are being victimized. In this example, the number of different serving pilot signals in the clusters areas, is so high (more than six) that it can not be identified which cell should provide service in that area.

In the following sections some detection results from a 4G network in an rural environment are presented. In Figure 5.5 the detection input parameters and the correspondent values used to obtain the detection results are detailed.

Table 5.5: 4G self-diagnosis detection parameters.

	CH	OS	PP
RSRP threshold [dBm]	-115	-100	-115
RSRP delta [dB]	3	6	10
Min RSRQ threshold [dB]	N/A	-10	N/A
RSRQ delta [dB]	N/A	6	6
Bins/Cluster [#]	10	10	10
Min inter-cluster distance [m]	57.5	57.5	57.5
Max serving cells	N/A	N/A	3

5.2.4   LTE - Coverage Holes

The first example is a coverage holes detection result in a rural area, see Figure 5.11.

As the previous detection results, the diagnosed cell is the blue cell with one cluster in coverage holes conditions. The detected cluster is composed by 23 bins and the blue cell average RSRP measured value is -121 dBm and an average value of RSRQ of -14 dB.

Using software with elevation profile capabilities, the terrain profile between the diagnosed cell and the coverage hole detected is presented in Figure 5.12. Even though the existence of LoS, due to the distance of approximately
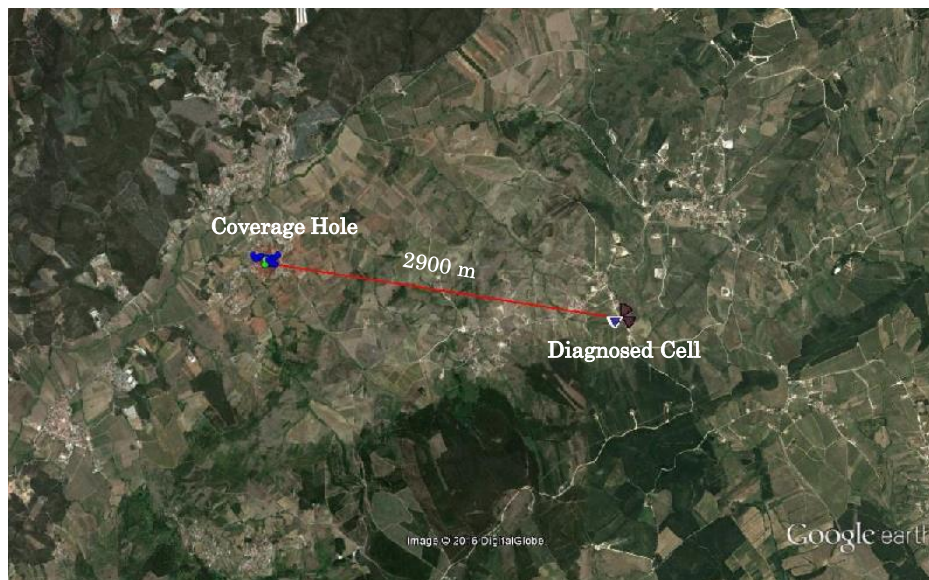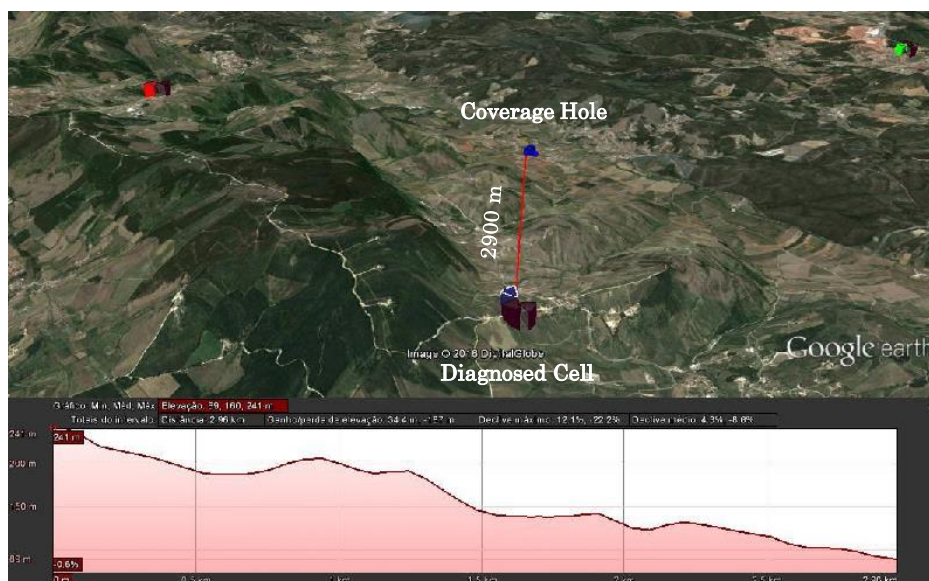
Figure 5.11: LTE coverage hole scenario.

Figure 5.12: LTE coverage hole cluster terrain profile.

3 km and mainly the MDT and EDT parametrizations of four and five degrees respectively, the received power is low, as seen. In addiction, the lack of cell dominance in the coverage cluster, led the algorithm to identify the green cell (top right corner of Figure 5.12) as a possible server for that area.

It can be concluded that is not clear which cell should provide service in that area and the optimization of the blue cell or the green cell could potentially minimize the lack of coverage.

Regarding the H_{cell} index, it returned a value of 4.76%. This asserts that the overall performance of the blue cell is good, as only 4.76% of its footprint evidences coverage holes.

5.2.5   LTE - Oveshooting

The second example is the overshooting detection result. Due to the distance between the diagnosed cell and the two overshooting clusters, around 15 km, it's more difficult to identify the cell and the clusters. Nevertheless, the diagnosed cell (blue) is in the upper part of Figure 5.13 connected with a red line to the first cluster.
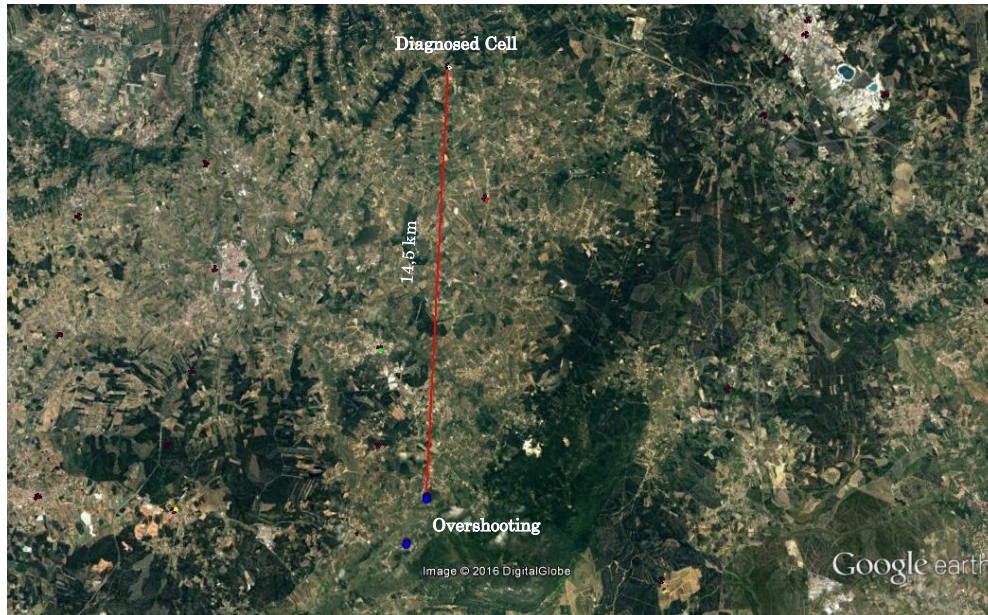

Figure 5.13: LTE overshooting scenario.

Two different clusters were detected far beyond the cell service area, where the blue cell in those cluster areas displays an average RSRP value of -91 dBm and an average value of RSRQ of -8 dB.

For additional information, Figure 5.14 exhibits the terrain profile between the blue cell and the first overshooting cluster.
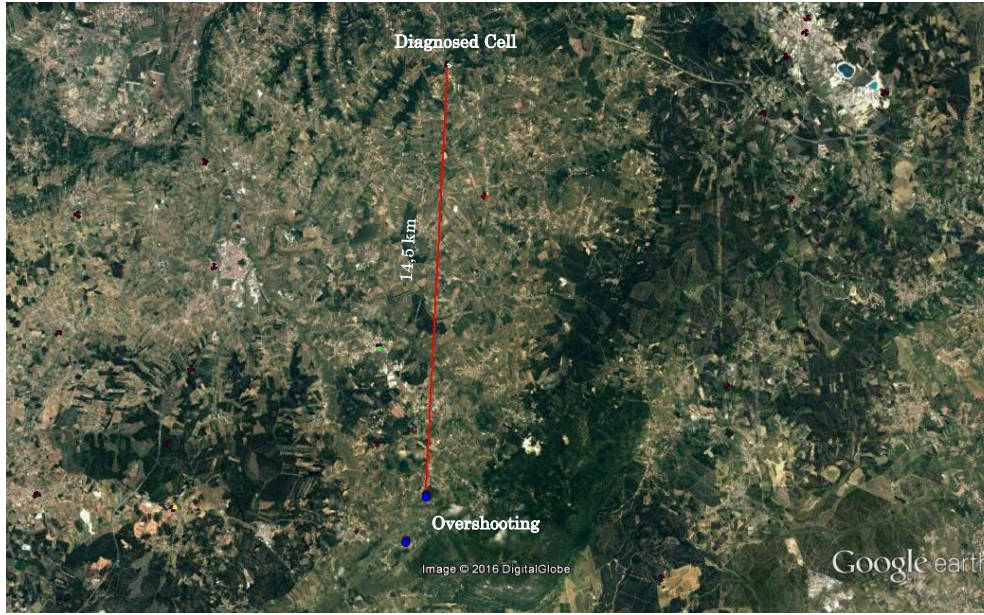
Figure 5.14: LTE overshooting cluster terrain profile.

The terrain profile evidences the existence of LoS, which enables the magnitude of the received power measured at this distance of 15 km. For one of the clusters, due to lack of cell dominance, it was unable to identify the victim cells. For the second cluster, two victim cells were identified, either one or another were located at inferior distances and with LoS granting good RF conditions.

In relation to the H_{cell} index value, it was 3%. It means that the average affected victim cells footprint was 3%.

5.2.6   LTE - Pilot Pollution

Relative to the pilot pollution results, an example is shown in Figure 5.15.

The diagnosed cell, with the blue color, in the inferior left corner is provoking pilot pollution in the upper part of Figure 5.15, between the green and the red cells. It was identified one cluster, where the dominant cells are the green and red cells, thus the color differentiation. The average RSRP value measured in the pilot pollution cluster was -103 dBm and an average RSRQ value of -22 dB. By the quality average value, the high level of interference can be ascertained.

Figure 5.15: LTE pilot pollution scenario.

Finally, in Figure 5.16 the terrain profile is presented.

Figure 5.16: LTE pilot pollution cluster terrain profile.

The diagnosed cell has LoS to the pilot pollution cluster, furthermore, its downtilt parameters (MDT and EDT) are set to zero degrees, each. This configuration enables to the reference signal to be propagated to other cells

service areas inducing interference. The H_{cell} index value was 2.96%, meaning
that, on average only 3% of the victim cell footprint was being affected.

5.3   Self-Optimization

Concerning the self-optimization algorithm, it was tested in the same urban
scenario with real data from a mobile operator. Using a smaller area that
contained 14 cells with either possible coverage, overshooting or pilot pol-
lution issues. All 14 cases, were optimized taking equally into account, the
three optimization targets above-mentioned, see Table 5.6. In 64% of the

Table 5.6: Cell self-optimization results.

Optimal Configuration [%]	64
Partial Configuration [%]	36
Average gain [%]	78

cases, it was found an antenna physical parameters configuration that min-
imized the objective function (Equation 4.17) to zero, in such a way that
the cell performance issues were solved. In 36% of the cases, the found so-
lution, was not optimal but improved the cell performance, according to the
objective function value. Taking into account that a gain of 100%, represents
an antenna configuration that minimizes the objective function to zero, the
average gain, for the cells optimized, was 78%.

In Figure 5.17 is presented a comparison between results before and after
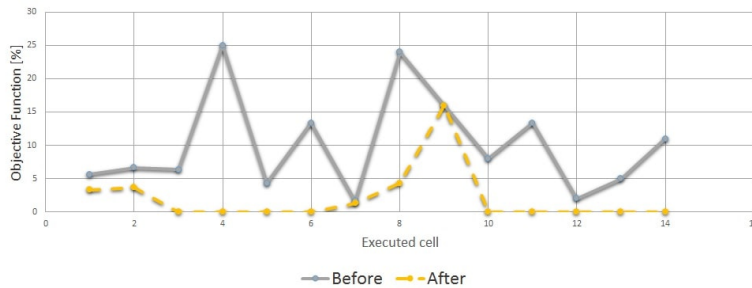optimization. The gray line represents the objective function value, for each

Figure 5.17: Comparison of antenna optimization results.

cell before optimization. Regarding the orange line, it indicates the objective
function values after the cell optimization. It can be ascertained that the
objective function values, which defines the low coverage and interference
severity, are reduced in the majority of the cases to values close to zero, that
represents an antenna configuration that solves the aforesaid cell problems.

In figure 5.18, it is represented an example of one optimized cell (blue)
and its footprint. As described in Section 4.4.3, the cell footprint is di-
vided in clusters for the optimization process. The ones highlighted with
the green color, identify the areas where the blue is dominant/co-dominant.
The remaining, identify areas that besides the cell reaching it, the cell is not
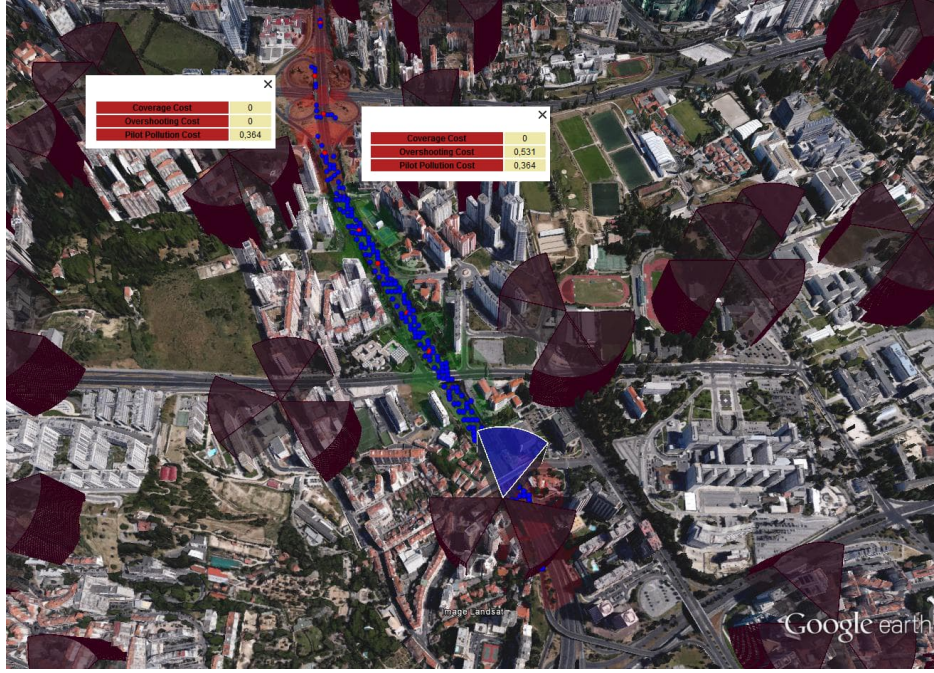dominant.

Figure 5.18: Cell footprint before optimization.

In this scenario, there were two clusters that according to Section 4.3,
the $H_{cluster}$ for overshooting and pilot pollution returned different than zero,
thus consisting of a pilot pollution and overshooting scenarios. The respective
$H_{cluster}$ values can be ascertained in Figure 5.18.

Afterwards, the self-optimization algorithm was executed and purposed
a new antenna configuration, presented in Table 5.7. The original antenna

Table 5.7: Antenna configurations comparison.

	Before Optimization	After optimization
EDT [º]	3	5
MDT [º]	2	7
C(Ω) [%]	5	0

configuration was set to three degrees of EDT and two degrees of MDT. Bearing in mind, that it was opted to not optimize the antenna orientation as it is not a typical primary optimization parameter, the self-optimization algorithm proposed an antenna configuration with five degrees of EDT and seven for the MDT, see Table 5.7.

The new antenna physical configuration increased both the MDT and the EDT, thus optimizing the cell. The applied downtilt reduced the received power in the initial problematic clusters, nonetheless it did not compromised the own cell service area in coverage matters.

The cell footprint measurements were estimated based on the new transmitter gain and its projection is illustrated in Figure 5.19.
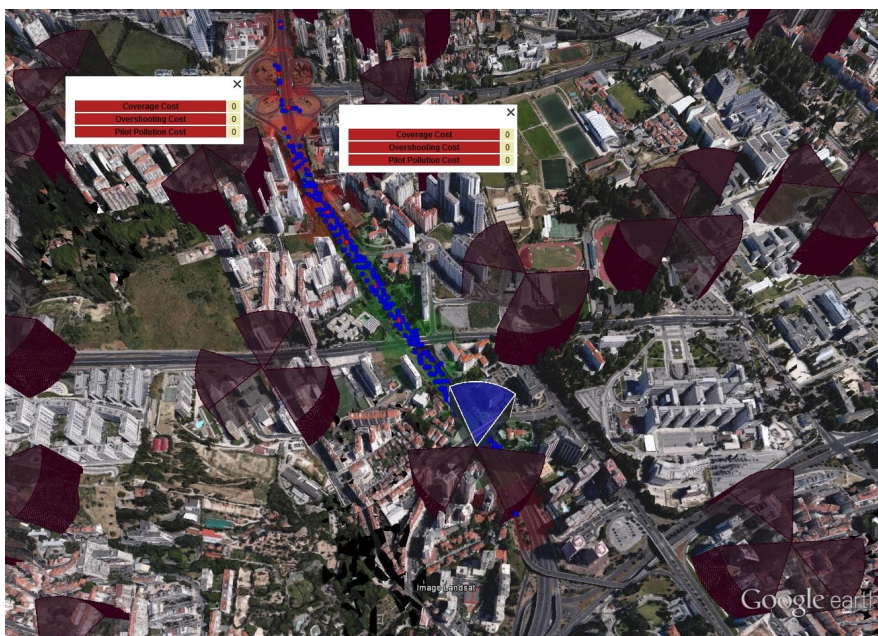

Figure 5.19: Cell footprint after optimization.

The simulated new DT RF measurements were recalculated according to Section 4.4.3. Firstly, it can be verified that the problematic clusters no longer exhibits neither overshooting nor pilot pollution. Secondly, this new antenna parameter configuration, diminishes the cell service area. This reduction does not impact network coverage, as the two clusters that previously belonged to the cell service area, corresponded to areas of cell co-dominance. This means that exists other cells reaching those clusters in RF conditions to provide service and the reduction of the cell service area does not impact negatively the network performance.

In Figure 5.20, an example of a DT bin containing the optimized cell measurement (blue) before and after the optimization is presented.
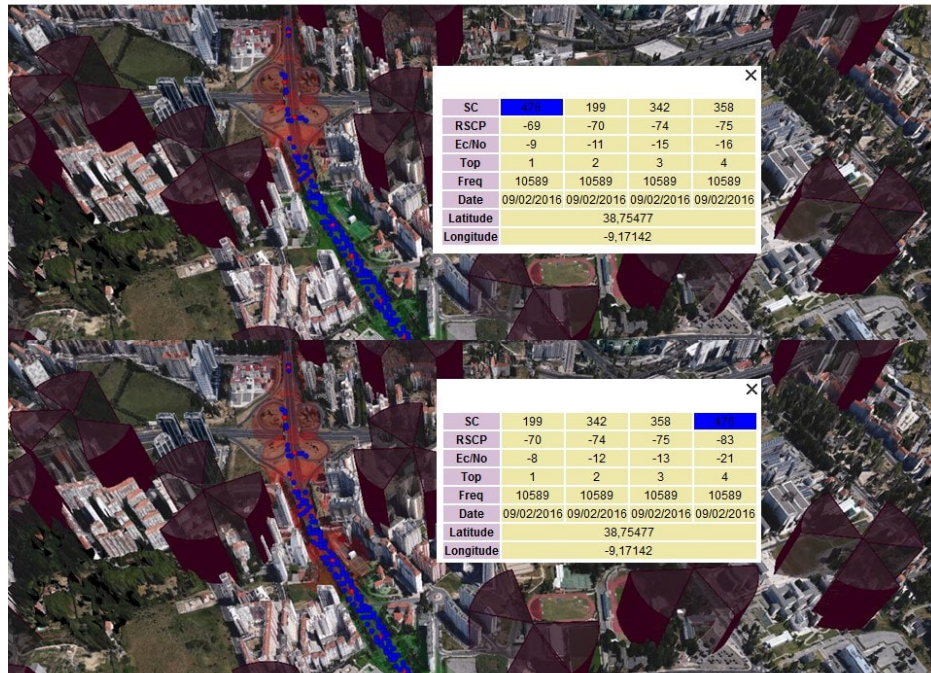

Figure 5.20: Simulated RF metrics.

The new antenna configuration, in the bin exhibited in Figure 5.20, reduced the received power in 14 dB. This power reduction, which was general in the affected area, allowed to eliminate the overshooting and pilot pollution scenarios. In addiction, it can be confirmed that other cells with good RF measurements grant good coverage and QoS to users in this area.

The cell optimization essentially deals with the trade off between maintaining good coverage in the cell service area diminishing interference in other cells service areas. An antenna physical parameter configuration that minimizes interference is only valid in case of being able to maintain coverage in the own cell service area. In that sense, Figure 5.21 show the Cumulative Density Function (CDF) of the power measurements before and after the optimization in the cell service area.
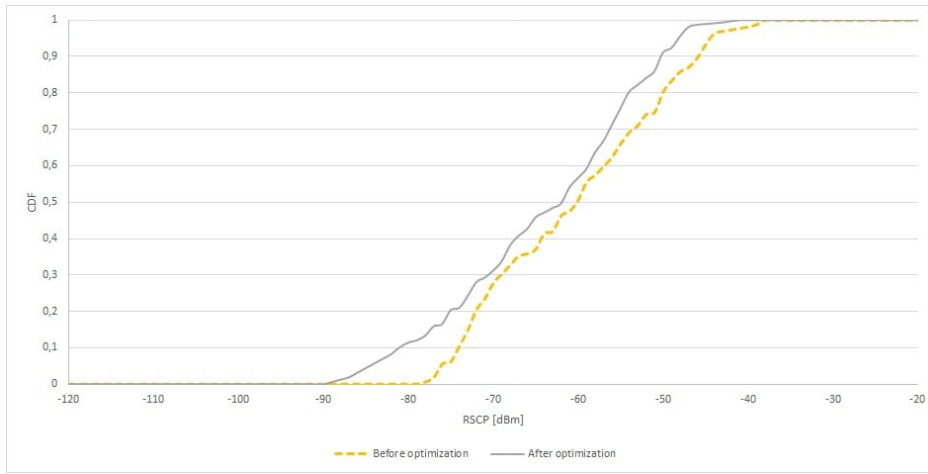

Figure 5.21: CDF of power in the cell service area.

As it can be seen, the power CDF before and after, are similar, which asserts that the new antenna configuration did not degraded the RF conditions in the cell service area. Analyzing more in depth Figure 5.21, it can be ascertained that the CDF after optimization reveals slightly lower power magnitude, nonetheless the new values still provide good coverage.

For the power CDF for the cell measurements collected outside the cell service area, ideally it should be as lower as possible. Figure 5.22 exhibits the CDF of the cell measurements located outside the cell service area, before and after the optimization.

While the 50% percentil of the power CDF before optimization was around -65 dBm, the equivalent 50% percentil after optimization was around -85 dBm. Which stands for a reduction of 20 dB. This magnitude reduction allowed to correct the interference issues of this cell.

Comparing the power CDF of the service area and the surrounding areas, it confirms that the power received outside the service area was reduced
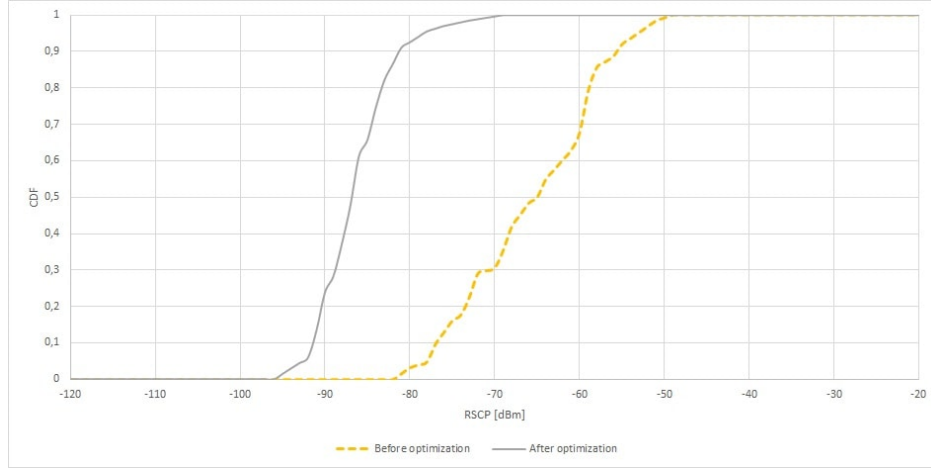
Figure 5.22: CDF of power outside the cell service area.

significantly, at the cost of a small power reduction in the cell service area. Which stands for a good trade off for the overall network performance.

Even though, the usage of DT data makes it easy to predict the cell RF metrics for different antenna configuration, which leads to an important drawback. It can only predict for the areas where the DT covered and collected measurements. On an automatic optimization feature based on this self-optimization algorithm, the extension and quality of the DT should be always validated previously to the optimization process using the above-mentioned DT reliability model, in the form of its reliability index R. This way, the optimized configuration, would have taken into account more data, and proposed a more reliable configuration.

In alternative, the usage of trace data, has an important advantage. Each iteration of a SON self-optimization feature, which consists on detecting RF performance issues and optimizing it through adjustment of the antenna physical parameters is limited by the timespan between acquiring new data. While using DT data, the timespan can be several days, by using trace data, the time resolution can be as small as fifteen minutes. This enables almost a real time monitoring and optimization of the network.

Chapter 6

Conclusions

This chapter briefly summarizes the findings and contributions of this thesis followed by future work directions.

6.1   Summary

In this master thesis work, it was developed a set of algorithms, that builds
the core of a network optimization SON feature, based on real DT or trace
data and real mobile operator network topology information.

On an automatic process, the ability to evaluate the quality of the avail-
able data is essential. Hence, it was developed a model to assess the DT
quality in a cell's coverage area, in the form of a DT reliability index. The
model is aware of road/street context and radio environment, allowing the
DT data being embedded in a spatial point process that evaluates positioning
and dispersion.

Based on the DT data (or trace data), a new approach for automatic
detection of low coverage and high interference scenarios (overshooting and
pilot pollution) in UMTS/LTE networks was developed. These algorithms
identify the problematic cluster locations and compute harshness metrics, at
cluster and cell level, quantifying the extent of the problem.

Furthermore, to optimize the detected network problems, it was consid-
ered a new single cell multi-objective antenna physical parameter optimiza-
tion algorithm. Based on DT measurements, the algorithm optimizes low
coverage and high interference by proposing a new tilt and antenna orienta-
tion (optional) values.

All algorithms were tested mainly in urban scenarios, where a MNO focus
its optimization efforts and where the optimization process is more complex.

In relation to the DT quality assessment model, it was tuned using sub-
jective testing by performing inquiries to fifty experienced radio engineers.
This enabled to calculate a more realistic DT reliability index supported by
professional experience.

Concerning the self-diagnosis algorithms (coverage holes, overshooting
and pilot pollution), the results showed that in urban areas and with a high
site density, the main optimization efforts rely on the interference mitigation
and not coverage optimization. Moreover, the pilot pollution scenarios were
the most prevalent.

The cluster division of the suboptimal data, using a RF correlation dis-
tance limitation, enabled a data grouping based on a certain level of correla-
tion of the respective radio channel. It provides a more accurate detection of
RF problems and a simplified framework for the antenna physical parameter

optimization algorithm.

The cell and cluster metrics, provide valuable information for the RAN engineers, in the sense that, they can target their efforts, firstly for the most damaging situations. Moreover, these values can be used as baselines in future optimization for results comparison and performance evaluation.

The self-optimization algorithm provided an average 78% gain for cells with detected RF problems. Bearing in mind that the optimization can only be set based on the available DT data (it might be insufficient) and that the self-optimization algorithm is self-aware of the surrounding cells, to prevent non intentional performance damages, the optimal antenna configuration is not achievable in every situation. Even though, with the prior constraints, in the cases where the optimal solution was not found, the algorithm minimized the previous detected problems.

6.2 Future Work

Future work is in motion by adding multi-cell multi-objective capabilities in the self-optimization algorithm. Further improvements are being considered, adding a hybrid optimization approach based on DT and calibrated radio propagation models to estimate RF metrics where the DT did not retrieve data.

Regarding the DT reliability algorithm and mainly the overshooting algorithm, the automatic service area definition based on the surrounding topology can be improved, by taking into account the terrain profile and considering a propagation model.

Finally, to complete a fully automatic SON feature, a method of parsing the results from the antenna self-optimization algorithm to the live network should be developed.

Bibliography

[1] 3rd Generation Partnership Project. 3gpp tr 36.814 v0.4.1(2009-02). Technical report, 3GPP, 2009.

[2] R.A. Dovich. *Quality Engineering Statistics*. ASQC Quality Press, 1992.

[3] Ericsson. Ericsson mobility report. Technical report, ERiCSSON, 2016.

[4] Amitabha Ghosh and Rapeepat Ratasuk. *Essentials of LTE and LTE-A*. Cambridge University Press, New York, NY, USA, 1st edition, 2011.

[5] Alan Julian Izenman. *Modern Multivariate Statistical Techniques: Regression, Classification, and Manifold Learning*. Springer Publishing Company, Incorporated, 1 edition, 2008.

[6] Heikki Kaaranen, Siamak Naghian, Lauri Laitinen, Ari Ahtiainen, and Valtteri Niemi. *UMTS Networks: Architecture, Mobility and Services*. John Wiley & Sons, Inc., New York, NY, USA, 2001.

[7] M.A. Kalkhan. *Spatial Statistics: GeoSpatial Information Modeling and Thematic Mapping*. Taylor & Francis, 2011.

[8] J. Korhonen. *Introduction to 4G Mobile Communications:*. Artech House mobile communications series. Artech House, 2014.

[9] P. Kyösti, J. Meinilä, L. Hentilä, X. Zhao, T. Jämsä, C. Schneider, M. Narandzić, M. Milojević, A. Hong, J. Ylitalo, V. Holappa, M. Alatossava, R. Bultitude, Y. Jong, and T. Rautiainen. Ist-4-027756 winner ii d1.1.2 v1.2. Technical report, EBITG, TUI, UOULU, CU/CRC, NOKIA, 2007.

[10] Xi Li. *Radio Access Network Dimensioning for 3G UMTS, First Edition (Advanced Studies Mobile Research Center Bremen)*. Vieweg+Teubner Verlag, San Francisco, CA, USA, 2011.

[11] Andrew Richardson. *WCDMA Design Handbook*. Cambridge University Press, New York, NY, USA, 2011.

[12] Matthew N. O. Sadiku. The handbook of ad hoc wireless networks. chapter Satellite Communications, pages 149–173. CRC Press, Inc., Boca Raton, FL, USA, 2003.

[13] S. S. Shapiro and M. B. Wilk. An Analysis of Variance Test for Normality (complete samples). *Biometrika*, 52(3-4):591–611, 1965.

[14] Yuhui Shi and Russell C. Eberhart. A Modified Particle Swarm Optimizer. In *Proceedings of IEEE International Conference on Evolutionary Computation*, pages 69–73, Washington, DC, USA, May 1998. IEEE Computer Society.

[15] Juan Sánchez-González, Oriol Sallent, Jordi Pérez-Romero, and Ramon Agustí. A multi-cell multi-objective self-optimisation methodology based on genetic algorithms for wireless cellular networks. *International Journal of Network Management*, 23(4):287–307, 2013.

[16] Satyobroto Talukder. Mathematicle modelling and applications of particle swarm optimization. Master's thesis, , School of Engineering, 2011.

[17] Agilent Technologies and Moray Rumney. *LTE and the Evolution to 4G Wireless: Design and Measurement Challenges*. Wiley Publishing, 2nd edition, 2013.

[18] Frans Van Den Bergh. *An Analysis of Particle Swarm Optimizers*. PhD thesis, Pretoria, South Africa, South Africa, 2002. AAI0804353.

[19] P. Vieira, N. Varela, N. Fernandes, N. Guedes, L. Varela, and N. Ribeiro. A son enhanced algorithm for observed time differences based geolocation in real 3g networks. In *Wireless Personal Multimedia Communications (WPMC), 2013 16th International Symposium on*, pages 1–5, June 2013.

[20] Ian H. Witten and Eibe Frank. *Data Mining: Practical Machine Learning Tools and Techniques, Second Edition (Morgan Kaufmann Series in Data Management Systems).* Morgan Kaufmann Publishers Inc., San Francisco, CA, USA, 2005.

[21] Nanning Zheng and Jianru Xue. *Statistical Learning and Pattern Analysis for Image and Video Processing.* Advances in Pattern Recognition. Springer, 2009.